

THESIS



This is to certify that the

thesis entitled

THE PREDICTION AND CORRELATION OF MODULI OF
POLYMER SOLUTIONS SUBJECTED TO LARGE
AMPLITUDE SHEAR OSCILLATIONS
presented by

Ekong A. Ekong

has been accepted towards fulfillment
of the requirements for

M.S. _____ degree in Chemical Engineering


Major professor

Date February 23, 1979



OVERDUE FINES:
25¢ per day per item

RETURNING LIBRARY MATERIALS:
Place in book return to remove
charge from circulation records

--	--

THE PREDICTION AND CORRELATION OF MODULI OF
POLYMER SOLUTIONS SUBJECTED TO LARGE AMPLITUDE
SHEAR OSCILLATIONS

By

Ekong A. Ekong

A THESIS

Submitted to

Michigan State University

in partial fulfillment of the requirements
for the degree of

MASTER OF SCIENCE

Department of Chemical Engineering

1979

ABSTRACT

THE PREDICTION AND CORRELATION OF MODULI OF
POLYMER SOLUTIONS SUBJECTED TO LARGE AMPLITUDE
SHEAR OSCILLATIONS

By

Ekong A. Ekong

A non-linear constitutive equation of Acierno et al. (1a) is tested on data of MacDonald et al. (1b), of stress generated in a 2% polyisobutylene solution in Primol 355, and subjected to a uniaxial oscillatory shear with finite amplitude. In fitting the data of MacDonald et al., the correct correlation of model results is strongly dependent on the adjustable parameter 'a'. The model quantitatively predicts a larger decrease (30%) of the dynamic storage modulus than of the dynamic viscosity (5%) up to a strain amplitude of 1.28 units, as observed by MacDonald. The model predicts only a slight dependence of both moduli on the frequency of oscillation in contrast to the Bird-Carreau model. At higher strain amplitudes, the undestroyed fraction of entanglement types corresponding to large relaxation times tend to the same value as in steady shear with equivalent shear rate. A qualitative agreement results in model prediction and shear stress growth data at large shear rates.

1a) D. Acierno et al., J. NonNewtonian Fluid Mech.,

Ekong A. Ekong

1, 125-146 (1976).

1b) I.F. MacDonald et al., Chem. Eng. Sci., 24,
1615-1625 (1969).

To my parents

ACKNOWLEDGMENTS

The author would like to express his sincere appreciation to Dr. K. Jayaraman for his guidance, assistance and exposure into the field of rheology, without which this work would have been impossible. Also his thanks goes to Drs. D. Acierno, G. Marrucci, G. Rizzo and G. Titomanlio all of Istituto di Ingegneria Chimica, Università de Palermo, Palermo (Italy) for their model; and Drs. I.F. MacDonald, J.D. Huppler, L.A. Holmes, E. Ashare, B.D. Marsh of the University of Wisconsin, Madison for the use of their experimental data.

TABLE OF CONTENTS

	Page
LIST OF TABLES	v
LIST OF FIGURES.	vi
INTRODUCTION	1
Background.	6
Small Amplitude Experiments	7
Large Amplitude Experiments	8
Stress Growth Experiments	10
The Constitutive Equation	12
The Acierno Model	12
The Bird-Carreau Model.	17
Determination of the Relaxation Spectrum.	18
Unsteady Shear Flow with Large Deformation.	22
Nonlinear Effects without Harmonics in Stress Signal	22
Determination of the adjustable parameter	27
Spectral analysis	34
The Structural Character in Oscillatory and Steady Shear.	39
Shear Stress Growth Prediction.	47
DISCUSSION	50
CONCLUSION	53
NOMENCLATURE	55
APPENDIX	58
REFERENCE.	70

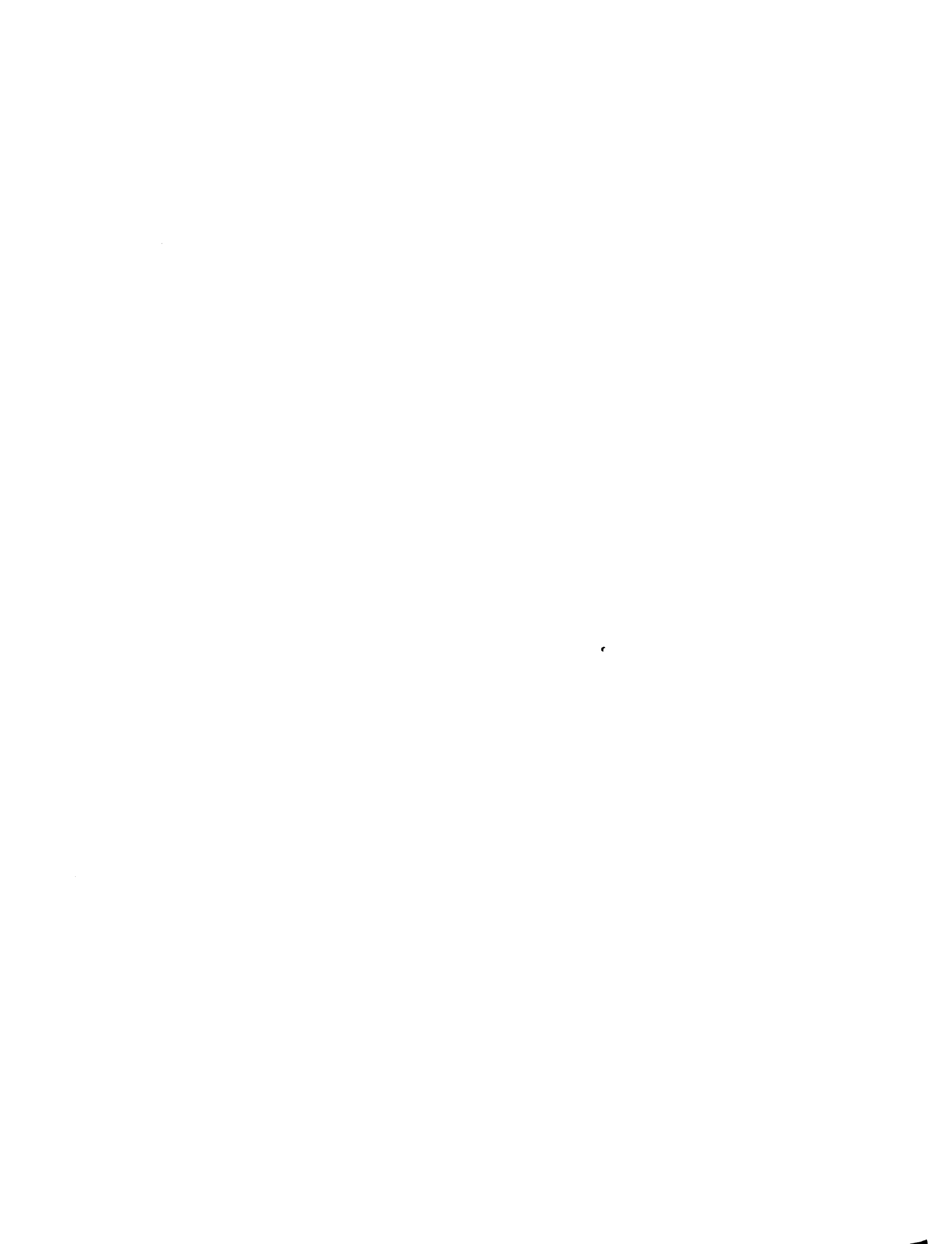
LIST OF TABLES

Table		Page
1	Contributions of different λ_0 regions to linear viscoelastic functions.	35
2	The effect of large amplitude on the different λ_0 region contributions to the nonlinear viscoelastic functions	37

LIST OF FIGURES

Figure		Page
1a	Small angle cone-and-plate viscometer.	2
1	The relaxation spectrum.	20
2	Steady and dynamic data of 2% polyisobutylene in Primol 355.	21
3a	Large amplitude dynamic viscosity data at $\omega = 0.188 \text{ sec}^{-1}$	28
3b	Large amplitude dynamic viscosity data at $\omega = 1.88 \text{ sec}^{-1}$	29
4a	Large amplitude storage modulus data at $\omega = 0.188 \text{ sec}^{-1}$	30
4b	Large amplitude storage modulus data at $\omega = 1.88 \text{ sec}^{-1}$	30
5	Large amplitude dynamic viscosity data with Acierno and Bird-Careau model predictions at $\omega = 0.188$ and 1.88 sec^{-1}	31
6	Large amplitude dynamic storage modulus data with Acierno and Bird-Carreau model predic- tions at $\omega = 0.188$ and 1.88 sec^{-1}	33
7	Spectral diagram of finite amplitude oscil- latory shear, $\gamma^0 = 0.2$, $\lambda_0 = 1.2 \text{ sec}$	41
8	Spectral diagram of finite amplitude oscil- latory shear, $\gamma^0 = 2.0$, $\lambda_0 = 1.2 \text{ sec}$	42
9	Spectral diagram of finite amplitude oscil- latory shear, $\gamma^0 = 2.66$, $\lambda_0 = 37 \text{ sec}$	43
10	The oscillatory and steady structural parame- ter, χ_j as a function of relaxation times. . .	45

Figure		Page
11	The oscillatory and steady structural parameter χ_j as a function of relaxation times and shear rate.	46
12	Shear stress and normal stress growth data and prediction for 2% polysiobutylene	48



INTRODUCTION

A number of useful properties and behavior of visco-elastic materials have been borne out of the classic small amplitude oscillatory shear experiments conducted by Ferry (1). Recently the Weissenberg Rheogonometer fitted with small angle cone and plate geometry as shown below has further enhanced the study of this flow regime on various classes of polymeric liquids.

First the polymeric solution is placed between the cone and plate. A sinusoidal motion of amplitude γ_0 is imposed on the cone while the plate is held steady and the gap between the platen and cone maintained constant. The sinusoidal strain input can be expressed as

$$\gamma_{\theta\phi} = \gamma^0 \sin \omega t \quad (1)$$

The torque on the plate and the axial force for constant gap between plate and cone are related to the tangential shear stress and first normal stress difference respectively

$$\tau_{\theta\phi} = \frac{3T}{2\pi R^3} \quad (2)$$

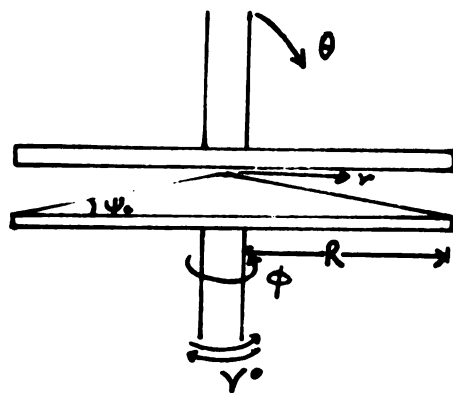


Figure 1a. Small angle cone-and-plate viscometer

$$N_1 = \tau_{\phi\phi} - \tau_{\theta\theta} = \frac{2F}{\pi R^2} \quad (3)$$

The determination of $\tau_{\phi\phi}$ and $\tau_{\phi\phi} - \tau_{\theta\theta}$ after the initial transients have died out through the equations above are obtained with the assumption that a linear velocity profile prevails within the gap. This assumption has been shown to be valid for small amplitude and small frequency motions (1b,2). The output stresses, $\tau_{\theta\phi}$, $\tau_{\phi\phi} - \tau_{\theta\theta}$ are observed to oscillate sinusoidally with frequency ω and 2ω of the input strain rate respectively (3). Also a phase shift is observed in the response functions. The input strain rate function and the stress responses can be represented as

$$\dot{\gamma}_{\theta\phi} = \text{Re} \{ \dot{\gamma}^0 e^{i\omega t} \} \quad (4)$$

$$\tau_{\theta\phi} = \text{Re} \{ \tau_{\theta\phi}^0 e^{i\omega t} \} \quad (5)$$

$$\tau_{\phi\phi} - \tau_{\theta\theta} = \text{Re} \{ (d_{\phi\phi} - d_{\theta\theta}) + (\tau_{\phi\phi}^0 - \tau_{\theta\theta}^0) e^{2i\omega t} \} \quad (6)$$

Using the theory of linear viscoelasticity (1) we define the material functions, the complex viscosity, η^* , the first normal stress difference displacement coefficient, θ_d , and the complex first normal stress-difference oscillation coefficient θ^* , as

$$\begin{aligned}\tau_{\theta\phi}^0 &= -\eta^* \dot{\gamma}_{\theta\phi}^0 = -(\eta' - i\eta'') \dot{\gamma}_{\theta\phi}^0 \\ d_{\phi\phi} - d_{\theta\theta} &= -\theta^d |\dot{\gamma}_{\theta\phi}^0|^2 \\ \tau_{\phi\phi}^0 - \tau_{\theta\theta}^0 &= \theta^* (\dot{\gamma}_{\theta\phi}^0)^2 = -(\theta' - i\theta'') \dot{\gamma}_{\theta\phi}^0{}^2\end{aligned}$$

These material functions often represent oscillatory flow properties of viscoelastic fluids and in the linear region are experimentally observed to be functions of the frequency of oscillation only.

It has been experimentally observed that if the amplitude γ^0 is increased, η^* , θ^d , θ^* become functions of the frequency as well as amplitude and linear viscoelastic theory no longer applies (1b). We therefore proceed to redefine large amplitude material functions as follows

$$\eta^*(\omega, \gamma^0) = \frac{\tau^0}{\dot{\gamma}^0} = \eta'(\omega, \dot{\gamma}^0) \quad (7)$$

$$\theta^d(\omega, \gamma^0) = - (d_{\phi\phi} - d_{\theta\theta}) / |\dot{\gamma}^0|^2 \quad (8)$$

$$\begin{aligned}\theta^*(\omega, \gamma^0) &= - (\tau_{\phi\phi}^0 - \tau_{\theta\theta}^0) / (\dot{\gamma}^0)^2 = \theta'(\omega, \gamma^0) - \\ &\quad - i\theta''(\omega, \gamma^0)\end{aligned} \quad (9)$$

Several constitutive equations have been proposed by rheologists (4) to appropriately relate the stress tensor through material functions to large deformation rates. These models centrally recognize the presence of nonlinear effects in the equation of motion and introduce a number of parameters to correctly predict the nonlinear

responses when large strain rates are imposed on polymeric fluids. Recently Acierno et al. (1a) proposed nonlinear constitutive equations based on the network molecular entanglement theory presented in detail by Lodge (5). This model was presented by the authors for polymeric melts and concentrated solutions with only a single adjustable parameter. It has also been used on polymeric solutions by Graessley et al. (6) for start-up and relaxation experiments.

The objective of this work is to test the predictive capability of the Acierno model in obtaining the material functions $\eta'(\omega, \gamma^0)$, $G''(\omega, \gamma^0)$, $\theta^d(\omega, \gamma^0)$ and $\theta^*(\omega, \gamma^0)$ that are to be determined experimentally by fellow workers (7) on the NBS fluid polyisobutylene in cetane. These experimental measurements are forthcoming and we turn to the literature data of McDonalds et al. (1b), who use 2% polyisobutylene in Primol 355. They collected $G'(\omega, \gamma^0)/G'(\omega)$ and $\eta'(\omega, \gamma^0)/\eta'(\omega)$ with $0.1 \leq \gamma^0 \leq 1.2$ at $\omega = 0.188, 1.88$ and 18.8 sec^{-1} . Also all data were taken at $25.0 \pm 0.1^\circ\text{C}$.

Our interest in this model stem from a) its successes in correctly predict various transient data reported by its authors (8) and Graessley et al. (6), b) the fewness of parameters and constants as compared with other models and c) the universality of the adjustable parameter in terms of flow regime and type of polymeric fluid as proclaimed by its authors.

Since the adjustable parameter 'a' is to be obtained through the guidance of dynamic shear data as opposed to steady shear as earlier suggested (8), we further evaluate 'a' by predicting the fluids start-up data of Huppler et al. (12). The Acierno model relates uniquely the relaxation times of the fluid to the existing entanglement density of network functions. By comparing the concentrations obtained through steady shear and averaged concentrations of the oscillatory data using the same 'a' value, we hope to ascertain some relationship between the shear rate $\dot{\gamma}$ and $\omega\gamma^0$ that has pervaded much of the literature.

Finally a brief comparison between the Bird-Carreau model and the Acierno model in their ability to predict $\eta'(\omega, \gamma^0)$ and $G'(\omega, \gamma^0)$ as a function of amplitude on the fluid under test will be presented.

Background

Many experimental rheologists have characterized the Non-Newtonian behavior of a number of polymeric fluids through steady shear experiments over two to three decades of shear rates. However the applicability of a constitutive equation to describe stress responses of Non-Newtonian fluids will depend on its ability to correlate other flow regimes as well. These flow regimes include start up and cessation of steady shear flow studied by Chen et al. (9) and Graessley (6), elongational flow experiments of Meissner (10), superposed steady and parallel/transverse oscillatory

shearing of Schowalter (11) and oscillatory shearing of McDonalds et al. (1b), and others (3,12). This list is by no means complete, each experimental set-up enabling the determination of the material function specific to the flow situation. In studying oscillatory shear flows it is necessary to review experimental and theoretical developments of small and large amplitude shearing as well as start-up experiments.

a. Small Amplitude Experiments

In the introductory paragraph, it was shown that small amplitude experiments enable the use of the theory of linear viscoelasticity and thus the characterization of fluids in terms of the material functions η^* , θ^d and θ^* . Furthermore the theory defines the linear viscoelastic functions listed above to be governed by the relaxation spectrum $H(\lambda)$ unique for each fluid (1) such that

$$\eta' = \int_{-\infty}^{\infty} \frac{H(\lambda) \lambda d \ln \lambda}{(1 + \omega^2 \lambda^2)} \quad (10)$$

$$G' = \int_{-\infty}^{\infty} \frac{H(\lambda) \omega^2 \lambda^2 d \ln \lambda}{1 + \omega^2 \lambda^2} \quad (11)$$

Also for small amplitude shear flow θ^* , and θ^d can be obtained directly from the following relations (4).

$$j\omega^* = \eta^*(\omega) - \eta^*(2\omega) \quad (12)$$

$$\omega \theta^d = \eta''(\omega) \quad (13)$$

which has been derived by a variety of viscoelastic models including Oldroyd three constant model (13).

Analogies have been presented both theoretically and experimentally between steady shear data and small amplitude oscillatory shear data and the most accepted is (14).

$$\eta_0 = \eta(\dot{\gamma})|_{\dot{\gamma} \rightarrow 0} = \eta'(\omega)|_{\omega \rightarrow 0} = H(\lambda) \lambda d \ln \lambda \quad (14)$$

$$\frac{\theta(\dot{\gamma})}{2\dot{\gamma}^2}|_{\dot{\gamma} \rightarrow 0} = \frac{G'(\omega)}{\omega^2}|_{\omega \rightarrow 0} = H(\lambda) \lambda^2 d \ln \lambda \quad (15)$$

In determining non-linear material functions, the small amplitude experiments will be useful if the non-linear viscoelastic model employed demands the dynamic linear properties of the fluid. In the Acierno model a relaxation spectrum is required and this can be obtained from the $\eta'(\omega)$ or $\eta''(\omega)$ vs ω data in the linear region through an inversion procedure (1).

b. Large Amplitude Experiments

Harris and Bogie (15) carried out finite amplitude oscillatory experiments on the Weissenberg Rheogonometer with a clear check that harmonics in the input signal were minimal. They observed for their different solutions, third and fifth harmonics in the stress amplitude as a function of frequency. Their polymer solution showed only a third harmonic in stress amplitude slightly sensitive to frequency while the fundamental harmonic was predominant.

Philippoff (16) using a rotational viscometer (conical arrangement) studied the effects of large amplitude up to 700% shear amplitude units on the material functions η' and G' of polymeric solutions. He noted that the largest third harmonic recorded in the recording system within the range of strain amplitude was not more than 5% of the amplitude of first harmonic in stress. He further observed decrease of G' and η' at higher strain amplitudes, G' decreasing considerably.

This experimental observations are consistent with linear viscoelasticity which recognizes a limiting amplitude beyond which the theory does not hold. So these data are in the realm of the non-linear models and along with other transient experiment can test the validity of the several proposed rheological equations of state. McDonalds et al. (16) working on three polymeric solutions of different composition and a melt studied the effect of large amplitude oscillatory shear on η' and G' . They obtained results similar to Phillipoff's and furthermore noted the effects were slightly dependent on the fluid and frequency of oscillation. They chose frequencies well within the power-law region of their four fluids. McDonalds data lends itself to comparative analysis with predictions of nonlinear models since they maintained a linear velocity profile in the input deformation. Tee and Dealy (17) also found from large amplitude oscillatory shear in a small gap concentric

cylinder rheometer that the extent of nonlinearity in the stress response is primarily a function of strain amplitude and independent of frequency. Strain amplitudes up to 10 and frequencies between 0.5 to 30 sec^{-1} were employed. In most of these studies inertial effects are neglected or compensated for. Dodge and Krieger (18) have argued that due to secondary flow, conventional analysis on oscillatory cone and plate geometry are not valid if fluid density is not considered. They thus elected to work with parallel plates or coaxial cylinders in their experiments (18). However Walters (22) noted that for relatively high viscosity liquids (low frequencies) little error is incurred due to inertial effects in using any of the available geometries.

c. Stress Growth Experiments

This experiments more popularly known as start-up experiments involve a sudden initiation of simple shearing at a certain shear rate on a fluid at rest. It has been experimentally observed (2,6,12) that the response shear stress, $\hat{\sigma}_1(\dot{\gamma}, t)$ and the normal stress difference $\hat{N}_1(\dot{\gamma}, t)$ are functions of the input steady shear rate as well as time. At low steady shear rate, $\hat{\sigma}_1$ and \hat{N}_1 increase monotonically to their steady state value. In this limit $\hat{\sigma}_1$ and \hat{N}_1 are said to be governed by linear viscoelastic properties and are obtainable through the relaxation spectrum for the fluid (6). As the shear rate is increased

the functions $\hat{\sigma}_1$ and \hat{N}_1 overshoot their steady state value; then in some cases an undershoot follows. The magnitude and time of overshoot has also been shown experimentally to be a function of shear rate. Huppler et al (12) working on three nonlinear models, OWFS, WJFLMB and the Spriggs 4-constant models showed these models to give varying results on stress growth prediction while agreeing closely in predicting steady shear and stress relaxation data. Graessley et al. (6) reviewed various models, the strain rate, relative strain, averaged rate and structural dependent models on their ability to predict start-up as well as cessation after steady shear data collected with a modified (stiffened) Weissenberg Rheogonometer R-17. They reported fundamental inconsistencies between both the strain rate and relative strain models with their data. For the structural model (Acierno's) they obtained a reasonable fit with their data only when they adjusted the structural parameter 'a' at each shear rate where 'a' also fits fairly the steady shear and normal stress data. All these studies point to the importance of stress growth experiments in evaluating rheological models. We intend to use 'a' obtained from large-amplitude shear data to predict start-up data especially at large shear rates. Such tests may reveal whether 'a' obtained through oscillatory shearing can portray a wide range of viscoelastic behavior.

The Constitutive Equation

The non-linear constitutive equation proposed by Acierno et al (1a) will be considered in this study. Acierno et al. report that their model adequately correlates data on tangential and normal stress growth in shear, stress growth in elongation and normal stresses in shear creep. The Bird-Carreau model (19) an integral nonlinear model studied by McDonald et al. (1a) will be presented on a comparative basis in the study of large amplitude dynamic complex functions. The Bird-Carreau model has received wide attention and interest as it correctly predicts complex viscosity, non-Newtonian viscosity in steady shear primary normal stress difference and stress relaxation data (19,20).

a. The Acierno Model

The model is given by

$$\tau = \sum_i \tau_i \quad (16)$$

$$\frac{\tau_i}{G_i} + \lambda_i \frac{\delta}{\delta t} \left(\frac{\tau_i}{G_i} \right) = 2\lambda_i \underline{D} \quad (17)$$

$$\frac{dx_i}{dt} = \left(\frac{1-x_i}{\lambda_i} \right) - \frac{ax_i}{\lambda_i} \sqrt{\frac{E_i}{G_i}} \quad (18)$$

$$G_i = G_{0i} x_i \quad \lambda_i = \lambda_{0i} x_i^{1.4} \quad (19)$$

where $\underline{D} = \frac{1}{2} (\underline{\nabla} \underline{v} + \underline{\nabla} \underline{v}^T)$

$$\text{and } \frac{\delta \tau_i}{\delta t} = \frac{d\tau_i}{dt} - \nabla_{\nu} \tau_i - \tau_i \nabla_{\nu}^T$$

The G_{0i} and λ_{0i} in equation (19) are the linear elastic moduli and relaxation times of the fluid respectively. These are obtained by the construction of the fluid relaxation spectrum $H(\lambda)$. The $H(\lambda)$'s are calculated from experimental curves of one of the three functions $G(t)$, $G'(\omega)$ or $G''(\omega)$ by an inversion procedure to be shown in section C. The $H(\lambda)$ vs λ plot is plotted on a log-log scale, then the $\log \lambda$ axis is subdivided into equal intervals $\Delta \log \lambda$. The mid-point of each sub-interval represent a set of discrete relaxation times λ_{0i} and the corresponding values of the ordinates H_{0i} gives

$$G_{0i} = H_{0i} \Delta \ln \lambda \quad (20)$$

Equation (19) relates elastic module G_i and the relaxation times λ_i to the existing structure through the structural variable x_i . Acierno et al. claim the set of x_i represent "the degree of connectivity of the macromolecular network with respect to that of equilibrium" (9). The rate of change of the variable x_i is given in equation (18) and is equal to the rate reformation of type i functions due to thermal motion minus the rate of destruction due to the existing stress. The destructive term is conceptively formulated by considering steady shear flow. In the absence

of thermal motion, n_j , the number of junctions of the i th type which on the average exist on the given molecule at any instant of time would be destroyed in a time of order $1/\dot{\gamma}$. Thus the rate of loss due to the imposed flow would be $an_j\dot{\gamma}$, where 'a' represents the ratio of a proper average contact time (attributed to thermal motions, entanglement property and other intrinsic properties) and its rough estimate $1/\dot{\gamma}$. Then the rate of junction loss relative to equilibrium junction concentration is given by $ax_j\dot{\gamma}$. In order to relate this term to the stress level γ is arbitrarily expressed in terms of the second invariant of the stress tensor during steady shear. This concept is further generalized to all flow histories. Equation (16) assumes that the total stress development of the fluid on a strain input is obtained by the superposition of all stresses induced by network junctions corresponding to relaxation times that contribute significantly at the time of consideration.

The model predicts zero second normal stress difference in shearing flows.

If unsteady oscillatory shear flows is considered, equation (11) predicts that except for τ^{12} and τ^{11} all other components of the extra stress remain zero.

Suppose

$$\underline{D} = \dot{\gamma} = \text{Re } \dot{\gamma}^0 e^{i\omega t}$$

Then
$$\frac{\tau_i^{12}}{G_i} + \lambda_i \frac{d}{dt} \left(\frac{\tau_i^{12}}{G_i} \right) = \lambda_i \operatorname{Re} \{ \dot{\gamma}^0 e^{i\omega t} \} \quad (21)$$

$$\frac{\tau_i^{11}}{G_i} + \lambda_i \frac{d}{dt} \left(\frac{\tau_i^{11}}{G_i} \right) = 2\lambda_i \left(\frac{\tau_i^{12}}{G_i} \right) \operatorname{Re} \{ \dot{\gamma}^0 e^{i\omega t} \} \quad (22)$$

$$\frac{dx_i}{dt} = \left(\frac{1-x_i}{\lambda_i} \right) - \frac{ax_i}{\lambda_i} \sqrt{\frac{\tau_i^{11}}{2G_i}} \quad (23)$$

By defining

$$\theta_i = t/\lambda_{0i}, \quad \alpha_i = a\lambda_{0i}\gamma^0 \quad (\gamma^0 \text{ assumed real}) \quad (23a)$$

$$T_i = \frac{a\tau_i^{12}}{G_i}, \quad N_i = \frac{a^2\tau_i^{11}}{G_i}, \quad \beta_i = \omega\lambda_{0i} \quad (23b)$$

eqns. (15) - (17) along with eqn. (13) become

$$T_i + x_i^{1.4} \frac{dT_i}{d\theta_i} = \alpha_i x_i^{1.4} \cos\beta_i \theta_i \quad (24)$$

$$N_i + x_i^{1.4} \frac{dN_i}{d\theta_i} = \alpha_i T_i x_i^{1.4} \cos\beta_i \theta_i \quad (25)$$

$$x_i^{1.4} \frac{dx_i}{d\theta_i} = 1 - x_i - x_i \sqrt{N_i} \quad (26)$$

The stresses σ^{12} and σ^{11} are continuous functions of time and can be represented by the sum of odd and even harmonics respectively by a Fourier expansion.

$$\text{i.e. } \tau_i^{12} = \sum_{n=0}^{\infty} \left[A'_{2n+1,i} \cos(2n+1)\omega t + B'_{2n+1,i} \sin(2n+1)\omega t \right] \quad (27)$$

$$\tau_i^{11} = C_{0i}' + \sum_{n=0}^{\infty} [D'_{2n+2,i} \cos(2n+2)\omega t + E'_{2n+2,i} \sin(2n+2)\omega t] \quad (28)$$

Also

$$\frac{\tau_i^{12}}{-\gamma^0} = \sum_{n=0}^{\infty} [A_{2n+1,i} \cos(2n+1)\omega t + B_{2n+1,i} \sin(2n+1)\omega t] \quad (29)$$

$$\frac{\tau_i^{11}}{-\gamma^0} = C_{0i}' + \sum_{n=0}^{\infty} [A_{2n+2,i} \cos(2n+2)\omega t + E_{2n+2,i} \sin(2n+2)\omega t] \quad (30)$$

From eqns. (7), (8), and (9)

$$\eta'(\omega, \gamma^0) = \sum_{i=1}^k A_{1i} \quad (31)$$

$$\eta''(\omega, \gamma^0) = G'(\omega, \gamma^0)/\omega = \sum_{i=1}^k B_{1i} \quad (32)$$

$$\theta^d(\omega, \gamma^0) = \sum_{i=1}^k C_{0i}', \quad \theta'(\omega, \gamma^0) = \sum_{i=1}^k D_{1i} \quad (33)$$

$$\text{and } \theta''(\omega, \gamma^0) = \sum_{i=1}^k E_{1i} \quad (34)$$

Solving the coupled equations (24), (25) and (26), $T_i(t)$ $N_i(t)$ for several values of t can be found. If 'a' has been predetermined, the sets

$$\left(\frac{\tau_i^{12}(t)}{-\gamma^0}, t \right)$$

and

$$\left(\frac{\tau_i^{11}(t)}{-\gamma^0}, t \right)$$

can be used to obtain the constants A_{2n+1} , B_{2n+1} , C_0 , D_{2n+2} and E_{2n+2} . At this point the predicted values of the amplitude of the various harmonics as well as the large amplitude material functions can be established.

b. The Bird-Carreau Model

The model is given by (28)

$$\tau = - \int_{-\infty}^{t'} \mu [t-t', \Pi(t')] \left\{ (1 + \frac{\epsilon}{2}) \underline{C}^{-1} + \frac{\epsilon \underline{C}}{2} \right\} dt' \quad (35)$$

with the memory function μ given by

$$\mu [t-t', \Pi(t')] = \sum_{n=1}^{\infty} \frac{\eta_n \exp[-(t-t')/\lambda_{2n}]}{\lambda_{2n}^2 [1 + 1/2 \Pi(t') \lambda_{1n}^2]} \quad (36)$$

where

$$\eta_n = \frac{\eta_0 \lambda_{1n}}{\sum_{p=1}^{\infty} \lambda_{1p}}, \quad \lambda_{jn} = \frac{\lambda_j^{2\alpha_j}}{(n+1)^{\alpha_j}} \quad j=1,2 \quad (37)$$

The terms η_0 , λ_1 , λ_2 , α_1 and α_2 are the model parameters determined from small amplitude oscillatory shear and steady shear experiments. The empirical constant ϵ allows for nonzero secondary normal stress difference. Further details of the model will not be presented here as they have been published elsewhere (1b,4,19,20).

In oscillatory shear motion McDonald et al. have derived $\eta^*(\omega, \gamma^0)$ for this model as

$$\eta^*(\omega, \gamma^0) = \sum_{n=1}^{\infty} \left\{ \eta_n A_n \frac{1 - i\omega \lambda_{2n}}{1 + \omega^2 \lambda_{2n}^2} \left[1 + \sum_{m=1}^{\infty} \binom{2m}{m} \left(\frac{B_n}{2} \right)^{2m} \right] - \right.$$

$$\sum_{n=1}^{\infty} \left\{ \frac{\eta_n A_n (1 - 2\omega^2 \lambda_{2n}^2 - 3i\omega \lambda_{2n})}{(1 + \omega^2 \lambda_{2n}^2)(1 + 4\omega^2 \lambda_{2n}^2)} \left[\sum_{m=1}^{\infty} \binom{2m-1}{m-1} \left(\frac{B_n}{2}\right)^{2m-1} \right] \right\} \quad (37a)$$

$$A_n = \frac{1}{(1 + 1/2 \lambda_{1n}^2 |\dot{\gamma}^0|^2)} \quad (37b)$$

$$B_n = 1/2 \lambda_{1n}^2 |\dot{\gamma}^0|^2 A_n \quad (37c)$$

This result assumes that no higher harmonics are observed in the stress response; $\eta'(\omega, \gamma^0)$ and $G'(\omega, \gamma^0)$ can be obtained from eqn. (37a).

c. Determination of the Relaxation Spectrum

The elastic moduli G_{0i} and relaxation times λ_{0i} 's encountered in the Acierno model can be determined through the construction of the relaxation spectrum $H(\lambda)$ which is obtained from the $G''(\omega)$ data. For 2% polyisobutylene in Primol 355 we used the $\eta'(G''/\omega)$ data of Huppler et al (28). An initial approximation of $H(\lambda)$ is made using Tschoegl's second approximation formula (1)

$$H_0(\lambda) = \frac{2}{\pi} \left(G''(\omega) - 4/3 \frac{dG'(\omega)}{d \ln \omega} + \frac{1}{3} \frac{d^2 G''(\omega)}{d(\ln \omega)^2} \right) \Big|_{\omega = 5/\lambda} \quad (38)$$

To obtain

$$\frac{dG''(\omega)}{d \ln \omega}$$

and

$$\frac{d^2 G''(\omega)}{d(\ln \omega)^2}$$

values, we fit the $G''(\omega)$ vs $\ln \omega$ data with a cubic spline, using the subroutine ICSVKU of the IMSL collection. ICSVKU starts with a given set of knots and shifts them among data points one by one in order to determine the knot locations that minimize the least square error. It then calculates the derivatives at the data points. More points were generated in the main program LSQSF within data limits for better precision in the next stage of $H(\lambda)$ determination.

Next, an iteration scheme was set up by comparing calculated values of $G''(\omega)$ and its observed values. From linear viscoelasticity,

$$G''(\omega) = \int_{-\infty}^{\infty} H_0(\lambda) \frac{\omega\lambda}{1+\omega^2\lambda^2} d\ln\lambda \quad (11)$$

Then

$$H_1(\lambda) = H_0(\lambda) [G''(\omega) \text{ obs} / G''(\omega) \text{ calc}]_{\omega=1/\lambda} \quad (39)$$

We failed to achieve convergence with the relationship $\omega = \sqrt{5}/\lambda$ as presented in equation (38). This relationship according to its author (21) represents a shift factor in the time scale at some point of the spectrum and was not fully understood. However on using the more conventional $\omega = 1/\lambda$ relationship, convergence was obtained after nine iterations. Then the ability of $H_1(\lambda)$ to reproduce

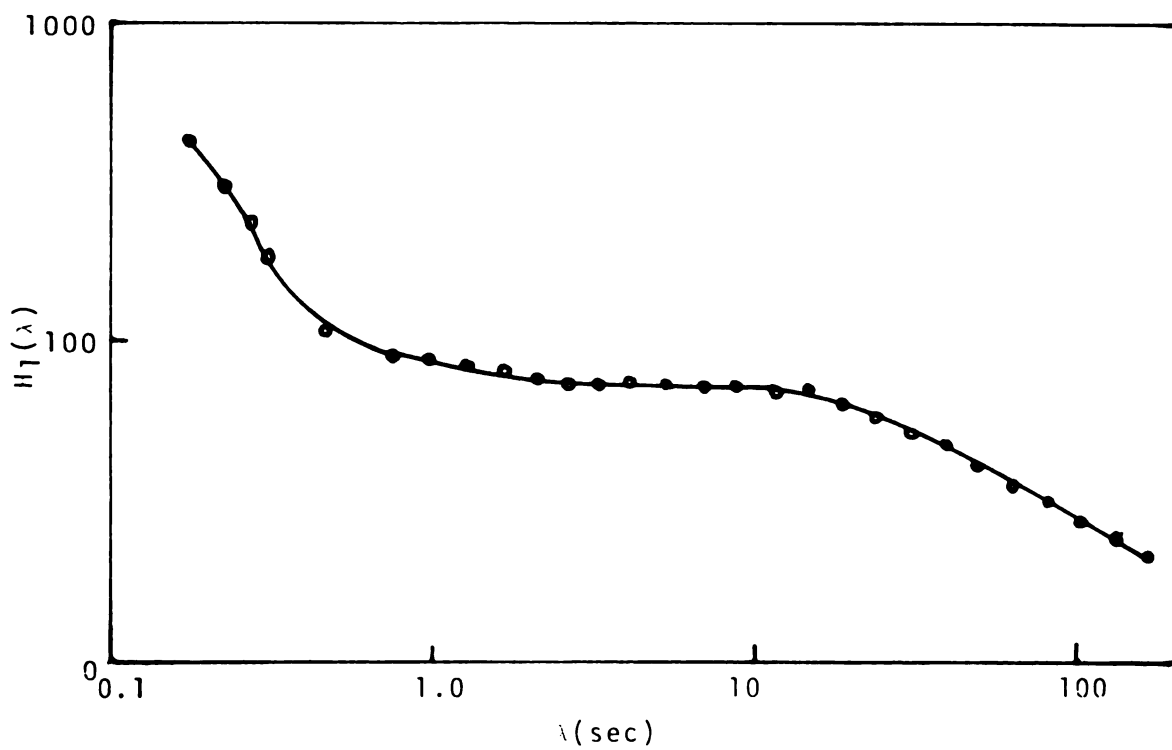


Figure 1. The relaxation spectrum calculated from $G''(\omega)$ (data of Huppler et al. (28)) for 2% polyisobutylene in Primol 355.

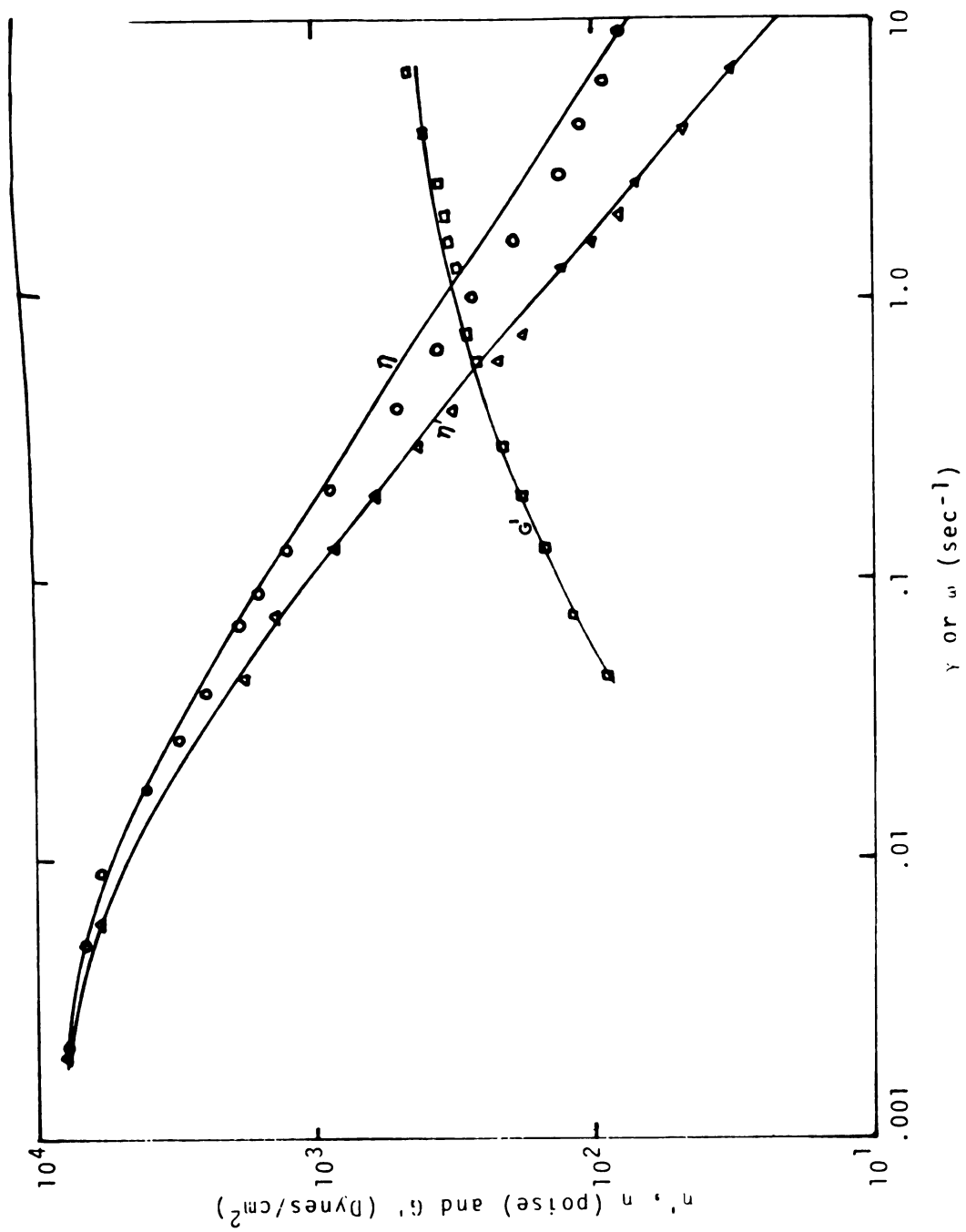


Figure 2. Steady and dynamic data of 2% polyisobutylene (Δ, \circ, \square , data from Huppler et al. (28) - G', n', n calculated from relaxation spectrum from Figure 1 (for $n = 0.3$))

linear data was further tested for the zero shear viscosity

$$\eta_0 = \int_{-\infty}^{\infty} H_1(\lambda) \lambda d \ln \lambda \quad (40)$$

The spectrum was then modified by successively removing the long relaxation times until an $\eta_0 = 10,350$ poise was obtained being a 4% error of the reported value (19). Using the procedure outlined in section A, fifteen G_0 and corresponding λ_0 values were obtained from the final spectrum shown in Figure 1. The longest relaxation time was 160 sec. The solid lines drawn through $\eta'(\omega)$ and $G'(\omega)$ data in figure 2 were calculated from this spectrum using the fifteen discrete G_0 's and λ_0 's mentioned earlier, using equations (10) and (11).

Unsteady Shear Flow with Large Deformation

In this section, we attempt to obtain the adjustment parameter 'a' of the Acierno model using a non-linear, transient flow experiment and evaluate its utility in terms of its ability to predict other characteristic behavior especially at large deformation rates.

a. Nonlinear Effects without Harmonics in Stress Signal

In large-amplitude oscillatory shearing experiments, using the cone and plate set-up we imply here that the imposed amplitude range is restricted such that only a

sinusoidal wave is recorded in the output torque measuring system. It can be assumed that in the Acierno model only the 1st harmonic of the dimensionless shear stress, T_i and the 2nd harmonic of the dimensionless Normal stress, N_i , and the average term of the structural measure x_i are significant.

Referring to eqns. (24) - (26)

Suppose

$$T_i = \alpha_i \text{Re} \{ T_{1i}^0 e^{i\omega t} \} \quad (41)$$

$$N_i = \alpha_i^2 \text{Re} \{ N_{20i}^0 + N_{22i}^0 e^{2i\omega t} \} \quad (42)$$

$$x_i = x_{i0} (\neq 1) \quad (43)$$

x_{i0} may be obtained from Eqn. (26)

$$1 - x_{i0} - \alpha_i x_{i0} \sqrt{N_{20i}} = 0$$

$$\text{where } \alpha_i = a\omega\lambda_{0i}\gamma^0$$

$$\text{i.e. } x_{i0} = \frac{1}{1 + \alpha_i \sqrt{N_{20i}}} \quad (43a)$$

$$\text{Now } (1 + \alpha_i \sqrt{N_{20i}})^{1.4} T_i + \frac{dT_i}{d\theta_i} = \alpha_i \cos \beta_i \theta_i \quad (43b)$$

$$(1 + \alpha_i \sqrt{N_{20i}})^{1.4} N_i + \frac{dN_i}{d\theta_i} = \alpha_i T_i \cos \beta_i \theta_i \quad (43c)$$

$$T_i = \alpha_i T_{1i} \cos(\beta_i \theta_i - \delta_{1i}); N_i = \alpha_i^2 (N_{20i} +$$

$$N_{22i} \cos(2\beta_i \theta_i - \delta_{2i}) \quad (43d)$$

$$\alpha_i (1 + \alpha_i \sqrt{N_{20i}})^{1.4} T_{1i} \cos(\beta_i \theta_i - \delta_{1i}) - \\ - \alpha_i \beta_i T_{1i} \sin(\beta_i \theta_i - \delta_{1i}) = \alpha_i \cos \beta_i \theta_i$$

or

$$T_{1i} [(1 + \alpha_i \sqrt{N_{20i}})^{1.4} \cos \delta_{1i} + \beta_i \sin \delta_{1i}] \cos \beta_i \theta_i \\ = \cos \beta_i \theta_i$$

$$T_{1i} = \frac{1}{(1 + \alpha_i \sqrt{N_{20i}})^{1.4} \cos \delta_{1i} + \beta_i \sin \delta_{1i}} \quad (44)$$

But

$$(1 + \alpha_i \sqrt{N_{20i}})^{1.4} \sin \delta_{1i} - \beta_i \cos \delta_{1i} = 0$$

$$\text{i.e. } \tan \delta_{1i} = \frac{\beta_i}{(1 + \alpha_i \sqrt{N_{20i}})^{1.4}} \quad (45)$$

From eqn. (43c)

$$\alpha_i^2 (1 + \alpha_i \sqrt{N_{20i}})^{1.4} [N_{20i} + N_{22i} \cos(2\beta_i \theta_i - \delta_{2i})] - 2\alpha_i^2 \beta_i N_{22i} \\ \times \sin(2\beta_i \theta_i - \delta_{2i}) = \alpha_i^2 T_{1i} \cos(\beta_i \theta_i - \delta_{1i}) \cos \beta_i \theta_i \\ = \alpha_i^2 T_{1i} \cos(2\beta_i \theta_i - \delta_{1i}) + \cos \delta_{1i}$$

From the time independent term

$$(1 + \alpha_i \sqrt{N_{20i}})^{1.4} N_{20i} = 1/2 T_{1i} \cos \delta_{1i}$$

$$N_{20i} = \frac{0.5}{(1 + \alpha_i \sqrt{N_{20i}})^{1.4} + \beta_i \tan \delta_{1i}}$$

$$\text{i.e. } N_{20i} = \frac{0.5}{(1 + \alpha_i \sqrt{N_{20i}})^{2.8} + \beta_i^2} \quad (46)$$

From the time dependent term

$$N_{22i} = \frac{1/2 T_{1i} \cos \delta_{1i}}{(1 + \alpha_i \sqrt{N_{20i}})^{1.4} \cos \delta_{2i} + 2 \beta_i \sin \delta_{2i}} \quad (47)$$

$$\text{where } \tan 2_i = \frac{\beta_i [2(1 + \alpha_i \sqrt{N_{20i}})^{1.4} + 1]}{(1 + \alpha_i \sqrt{N_{20i}})^{1.4} - 2 \beta_i^2} \quad (48)$$

With finite γ^0

$$\tau_{12} = (\eta'(\omega, \gamma^0) \cos \omega t + \eta''(\omega, \gamma^0) \sin \omega t) \omega \gamma^0$$

From model

$$\tau_{12} = \sum_i \frac{G_i T_i}{a} = \sum_i^2 G_{0i} x_i T_{1i} (\cos \omega t - \delta_{1i})$$

Therefore

$$\eta'(\omega, \gamma^0) = \sum_i \frac{G_{0i} \lambda_{0i} (1 + \alpha_i \sqrt{N_{20i}})^{0.4}}{(1 + \alpha_i \sqrt{N_{20i}})^{2.8} + \omega^2 \lambda_{0i}^2} \quad (49)$$

$$G'(\omega, \gamma^0) = \eta''(\omega, \gamma^0) \omega = \sum_i \frac{G_{0i} \omega^2 \lambda_{0i}^2}{(1 + \alpha_i \sqrt{N_{20i}})^{3.8} + (1 + \alpha_i \sqrt{N_{20i}}) \omega^2 \lambda_{0i}^2} \quad (50)$$

Also

$$\tau^{11} - \tau^{22} = \left[\theta^d(\omega, \gamma^0) + \theta'(\omega, \gamma^0) \cos 2\omega t + \theta''(\omega, \gamma^0) \sin 2\omega t \right] \omega^2 \gamma^0{}^2$$

From Model

$$\begin{aligned} \tau^{11} - \tau^{22} &= \sum_i \frac{2G_i N_i}{a^2} \\ &= 2 \sum_i G_{0i} x_i \alpha_i^2 |N_{20i} + N_{22i} (\cos 2\omega t - \delta_{2i})| \end{aligned}$$

i.e.

$$\theta^d(\omega, \gamma^0) = \sum_i \frac{G_{0i} \lambda_{0i}}{(1 + \alpha_i \sqrt{N_{20i}})^{3.8} + (1 + \alpha_i \sqrt{N_{20i}}) \omega^2 \lambda_{0i}^2} \quad (51)$$

and

$$\theta'(\omega, \gamma^0) = \sum_i \frac{G_{0i} \lambda_{0i} x_i}{\left[(1 + \alpha_i \sqrt{N_{20i}})^{2.8 + \beta_i^2} \right] \left[(1 + \alpha_i \sqrt{N_{20i}})^{1.4 + 2\beta_i \tan \delta_{2i}} \right]} \quad (52)$$

$$\theta''(\omega, \gamma^0) = \sum_i \frac{G_{0i} \lambda_{0i} x_i \tan \delta_{2i}}{\left[(1 + \alpha_i \sqrt{N_{20i}})^{2.8 + \beta_i^2} \right] \left[(1 + \alpha_i \sqrt{N_{20i}})^{1.4 + 2\beta_i \tan \delta_{2i}} \right]} \quad (53)$$

From Eqns. (50) & (51)

$$\theta^d(\omega, \gamma^0) = G'(\omega, \gamma^0) / \omega^2 \quad (54)$$

i. Determination of the adjustment parameter

The determination of $\eta'(\omega, \gamma^0)$, $\eta''(\omega, \gamma^0)$, $\theta^d(\omega, \gamma^0)$ $\theta^*(\omega, \gamma^0)$ as given in the preceding equations can be obtained only if 'a' is known. Since 'a' is a non-linear characteristic of the model we elected to correlate these material functions with experimental data and thus obtain an 'a' that gives the best fit. If an 'a' can simultaneously fit four non-linear material functions data, then its suitability for application to other flow histories over that obtained from steady shear data is justified. Unfortunately the Normal stress data for polyisobutylene are unavailable, and we use $\eta'(\omega, \gamma^0)$ and $G'(\omega, \gamma^0)$ data of McDonalds et al. (1b) for correlation.

The material functions $\eta'(\omega, \gamma^0)$ and $G'(\omega, \gamma^0)$ as functions of γ^0 are calculated using equations (49) and (50). The dimensionless Normal stress, N_{20j} , present in these equations is determined using equation (46), by a successive approximation procedure using its linear value as an initial estimate at all the relaxation times. The program LAMVIS presented in the Appendix reads in an arbitrary 'a' value and outputs the normalized $\eta'(\omega, \gamma^0)$ and $G'(\omega, \gamma^0)$ values as shown in Figures 3a - 5.

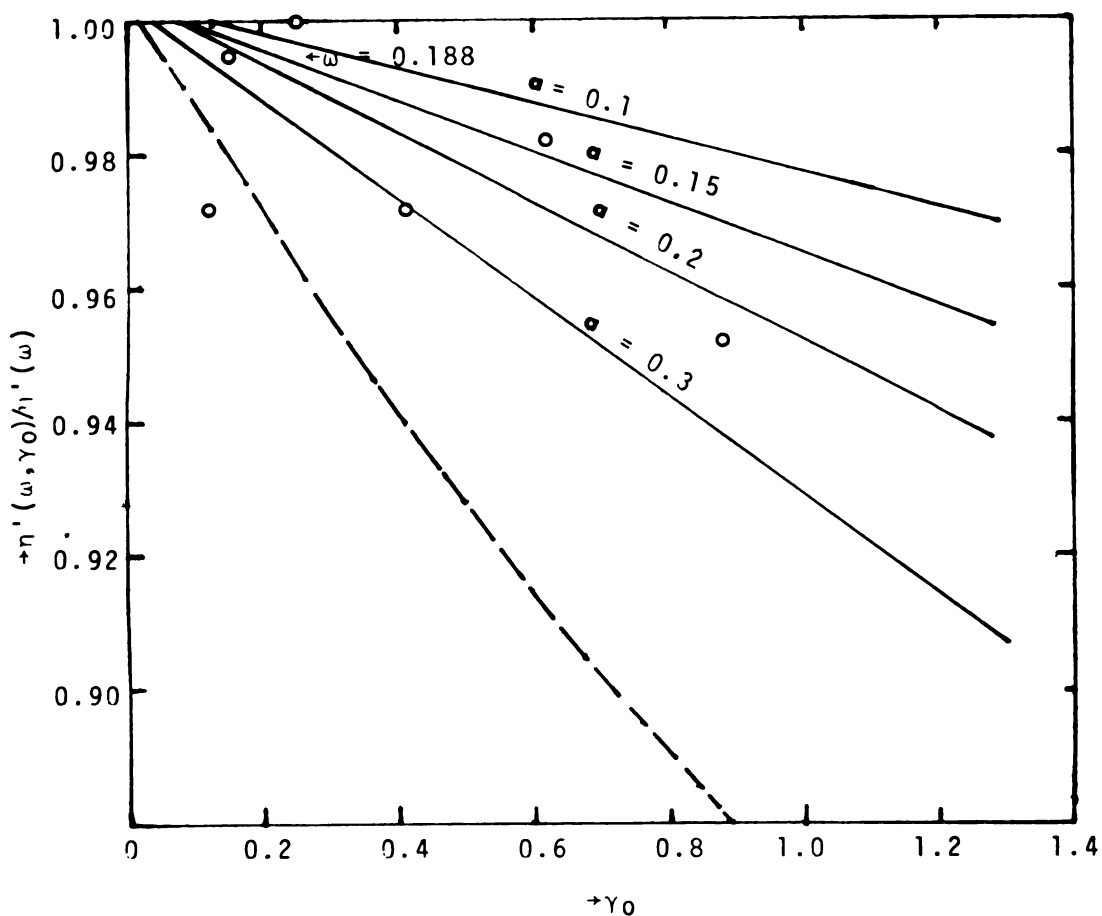


Figure 3a. Large amplitude dynamic viscosity data for 2.0 wt % PIB MD-237 in Primol.

— Acierno model
 - - - Bird-Carreau model
 O Data pts. $\omega = 0.188$ sec⁻¹
 (MacDonald et al.)

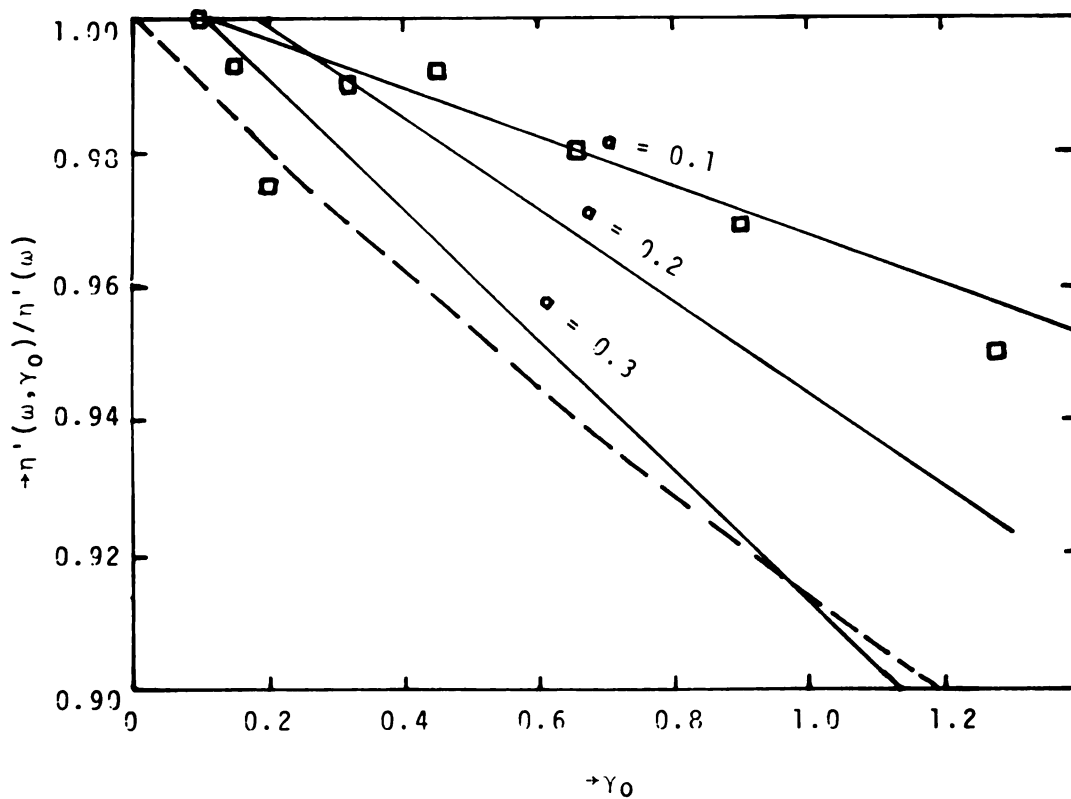
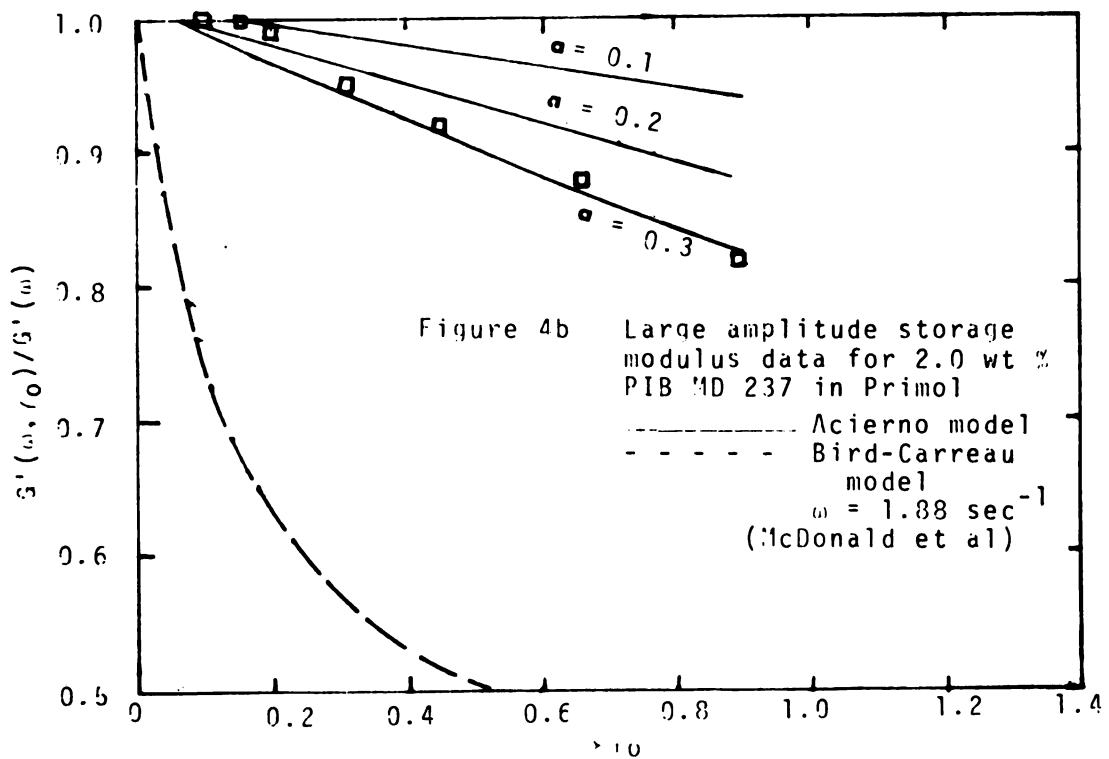
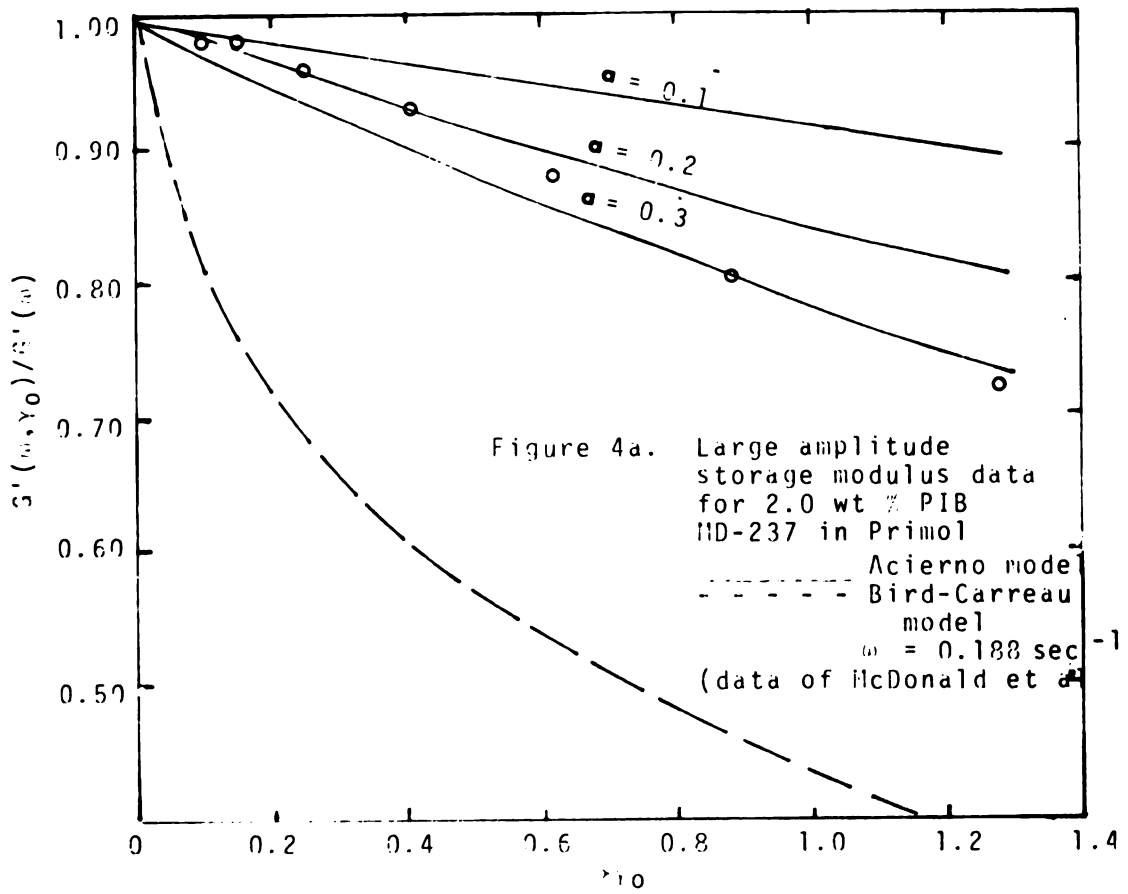


Figure 3b. Large amplitude dynamic viscosity data for 2.0 wt % PIB MD-237 in Primol

————— Acierno model
 - - - - - Bird-Carreau model
 Data pts. $\omega = 1.88 \text{ sec}^{-1}$
 (McDonald et al.)



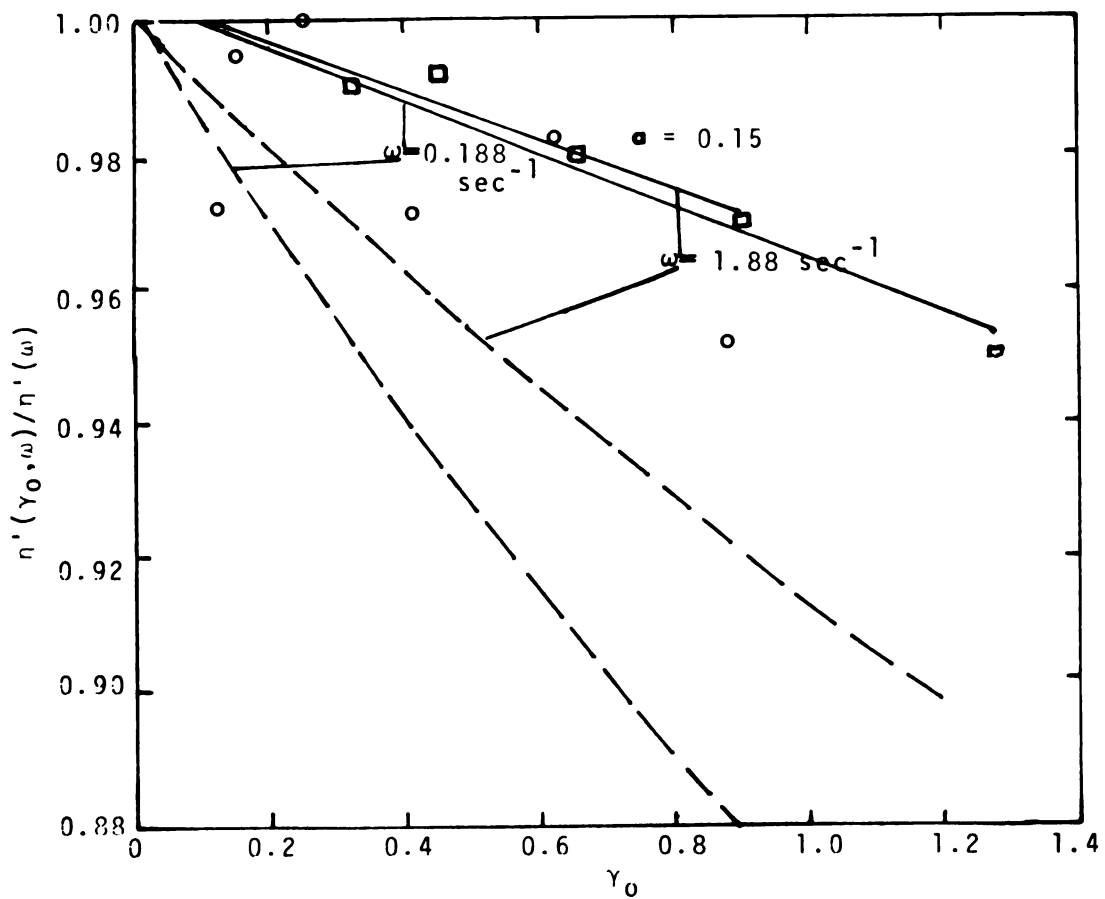


Figure 5. Large amplitude dynamic viscosity data for 2.0 wt% PIB MD-237 in Primol

————— Acierno model
 - - - - - Bird-Carreau model
 $\omega = 0.188 \text{ sec}^{-1}$
 $\omega = 1.88 \text{ sec}^{-1}$
 (MacDonald et al.)

In figures 3a and 3b the smooth curves are model predictions obtained for three values of 'a'. In contrast to Acierno results on steady shear data (8) the model slopes exhibits a strong sensitivity on the choice of 'a'. In the light of the scatter of experimental data it seems that an $0.1 \leq a \leq 0.15$ reproduce data well. Figure 5 shows a slight dependence of $\eta'(\omega, \gamma^0)/\eta'(\omega)$ predicted by the model on the frequency within the range of γ^0 studied. This seems to be supported well by the data and the same phenomenon has been reported by Philippoff (16). The dashed lines of Figure 5 are predicted values of the Bird-Carreau model and they exhibit a strong dependency on the frequency.

In figures 4a and 4b more drastic decrease of $G'(\omega, \gamma^0)/G'(\omega)$ as functions of γ^0 and 'a' is observed. Once again the model predictions show a strong dependence on the parameter 'a'. From Figure 6 the curve with $\alpha = 0.3$ gives the best prediction of the data at both frequencies. Since $G'(\omega, \gamma^0)/G'(\omega)$ data shows more reproducibility and more non-linearity, the 'a' obtained here has been chosen as more representative of nonlinear character of the fluid over that obtained from the $\eta'(\omega, \gamma^0)/\eta'(\omega)$ data.

This approximated form of Acierno model gives a relation between the first normal stress displacement and the dynamic storage modulus similar to the rheological relations of linear viscoelasticity. Walters (14) analyzing the effect of nonlinearity on dynamic normal stress behavior, however neglecting the fourth harmonic came up with a

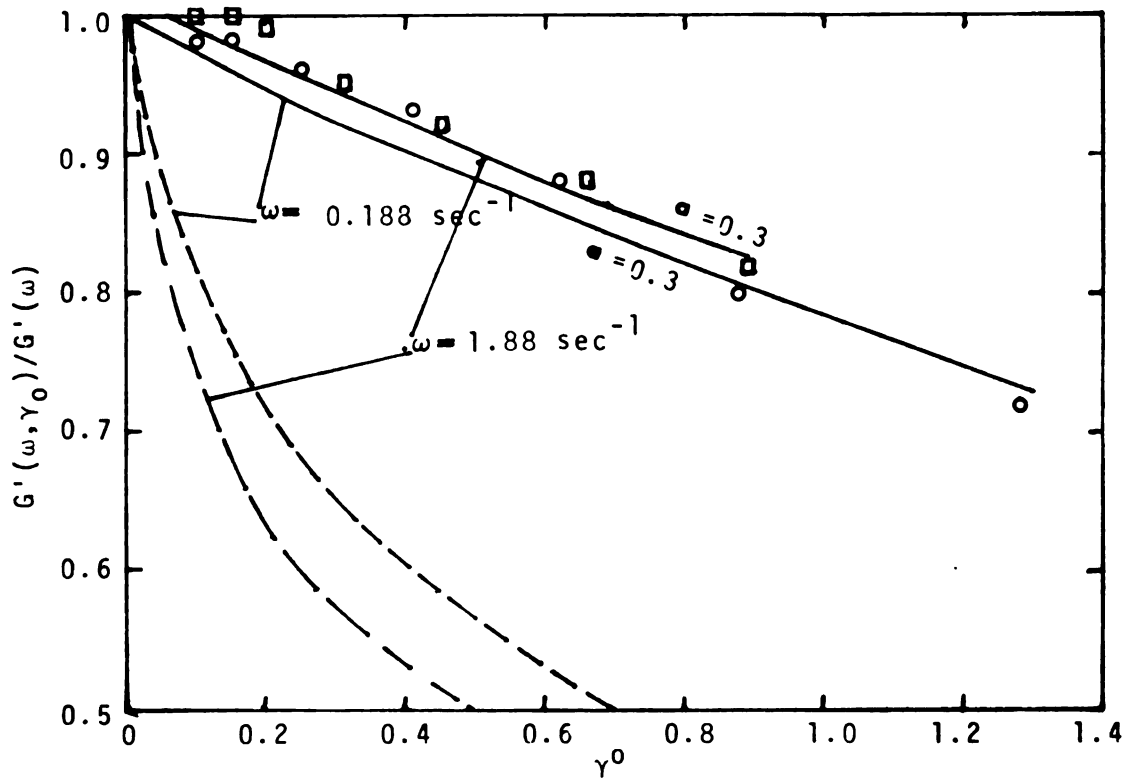


Figure 6. Large amplitude storage modulus data for
2.0 wt % PIB MD-237 in Primol

————— Acierno model
 - - - - - Bird-Carreau model
 $\omega = 0.188 \text{ sec}^{-1}$
 $\omega = 1.88 \text{ sec}^{-1}$

similar conclusion for both $\theta'(\omega, \gamma^0)$ and $\theta^d(\omega, \gamma^0)$. Christiansen and Leppard (3) also report a fair agreement on both the rheological relations when using $\gamma^0 = 0.743$ on their fluids. However this author feels that there is still merit in collecting data for oscillatory normal stress functions since it may serve as a critical test for correlating oscillatory nonlinearities. The Acierno model proposed the rate of destruction of the network junctions as a functional of the invariant of the normal stress which also carries the adjustment factor. Thus the correlation of this argument especially at high γ^0 in the oscillatory mode would be very significant.

ii. Spectral analysis

In Table 1 we categorize the relaxation spectrum into three broad spectral zones in the contribution of the $\eta'(\omega)$ and $G'(\omega)$ values. Much of the $\eta'(\omega)$ value is contributed by the $\omega\lambda \sim 1$ region, the $\omega\lambda \gg 1$ region giving the least contribution. In the $G'(\omega)$ data the $\omega\lambda \sim 1$ region contributes significantly but the greatest contribution comes from the $\omega\lambda \gg 1$ region. In Table 2 the network concentrations, x_i , of the different spectral zones are presented due to the imposition of the strain amplitude of $\gamma^0 = 0.41$ on the fluid. We observe the maximum effect of this large strain amplitude at the large relaxation times as x_i s in the $\omega\lambda \gg 1$ region deviate more from unity than those of smaller relaxation times. In other words the model

Table 1. Contributions of different λ_0 regions to linear viscoelastic functions

	$\omega = 0.188 \text{ sec}^{-1}$			$\eta'(\omega) = 640 \text{ poise}$			$G'(\omega) = 178 \text{ dyne/cm}^2$								
	$\omega\lambda \ll 1$			$\omega\lambda \sim 1$			$\omega\lambda \gg 1$								
λ_0 (sec)	0.17	0.28	0.46	0.74	1.2	2.0	3.2	5.2	8.6	14.0	23.0	37.0	60.0	98.0	160
$\omega\lambda_0$.032	.053	0.086	0.139	0.226	0.376	0.602	0.978	1.617	2.63	4.32	6.96	11.28	18.42	30.1
G'_i (%)	-	-	0.22	0.36	1.13	2.69	5.62	10.05	14.9	17.03	15.69	13.1	10.48	8.07	-
η'_i (%)	6.04	4.75	3.89	4.95	7.42	11.48	13.8	15.2	13.61	9.59	5.43	2.78	1.37	0.648	.314

predicts that the effect of non-linearity is restricted to larger relaxation times in the oscillatory flow regime.

Since $\eta'(\omega)$ is principally susceptible to the changes up to $\omega\lambda \sim 1$ region, the model predicts that the effect of nonlinearity in oscillatory shear will be least apparent through this material function. On the other hand the model predicts a drastic effect on the $G'(\omega)$ value since the zone $\omega\lambda \gg 1$ which gives the greatest contribution has been mostly affected. These two observations are correctly supported by McDonalds data.

Furthermore, we notice that in Table 2 in the $\omega\lambda \gg 1$ region there is a percent increase in $\eta'_i(\omega, \gamma^0)$ spectral contribution. This seems to be borne out of equation (49). If 'a' is chosen such that the nonlinear term $1 + a\gamma^0 \beta_i \sqrt{N_{20i}}$ is close to unity then the decrease of each spectral unit will be moderate. However if $\omega\lambda \gg 1$ then the denominator becomes

$$(1 + a\gamma^0 \beta_i \sqrt{N_{20i}})^2 + \omega^2 \lambda_{0i}^2 \doteq (\omega \lambda_{0i})^2$$

and

$$\frac{\eta'_i(\omega, \gamma^0)}{\eta'_i(\omega)} \geq 1 \quad (55)$$

But no significant increases was incurred as shown in Table 2. In sum the model verifies McDonald's assertion

Table 2. The effect of large amplitude on the different λ_0 region contributions to the nonlinear visco-elastic functions

	$\omega = 0.188 \text{ sec}^{-1}$ $\gamma^0 = 0.41$			$G'(\omega, \gamma^0) = 168.0 \text{ dyne/cm}^2$											
	$\eta(\omega, \gamma^0) = 631.82 \text{ poise}$			$G'(\omega, \gamma^0)/G'(\omega) - 1 = 0.056$											
	$\eta(\omega, \gamma^0)/\eta'(\omega) - 1 = -0.012$														
	$\omega\lambda < 1$			$\omega\lambda \sim 1$			$\omega\lambda > 1$								
$\lambda_0 t(\text{sec})$	0.17	0.28	0.46	0.74	1.2	2.0	3.2	5.2	8.6	14	23.0	37.0	60.0	98.0	160
$\lambda_1 t(\text{sec})$	0.17	0.28	0.46	0.74	1.2	2.0	3.1	5.0	8.2	13.2	21.7	34.9	56.5	92.3	150.5
$\omega\lambda_1 t$.032	.053	.086	.139	0.226	.376	.582	.94	1.54	2.48	4.08	6.56	10.6	17.4	28.3
x_1	.999	.998	.996	.994	.990	.985	.978	.971	.964	.961	.959	.959	.958	.958	.957
$\left(\frac{G_1'(\omega, \gamma^0)}{G_1'(\omega)} - 1\right)(\%)$	-	-	-2.75	-4.29	-6.56	-9.6	-12.2	-13.1	-11.9	-10.1	-9.0	-8.4	-8.2	-1.8	-
$\left(\frac{\eta_1'(\omega, \gamma^0)}{\eta_1'(\omega)} - 1\right)(\%)$	-0.33	-0.55	-1.2	-1.4	-2.1	-3.0	-3.6	-3.1	-1.4	+0.11	+1.03	+1.4	+1.6	+1.7	+1.8

that in nonlinear oscillatory shearing experiments, more emphasis should be given to $G'(\omega, \gamma^0)$ data rather than the $\eta'(\omega, \gamma^0)$ counterparts.

In Acierno's paper (8) it was shown that there was a drastic truncation of the relaxation spectrum during steady shearing experiments when shear rate as low as $\dot{\gamma} = 0.01$ was imposed. Also an $a = 0.4$ gave the best fit of their viscosity and first normal stress coefficient results. In Table 2 truncation of the right part of the relaxation spectrum was less drastic as the greatest change in λ_{0j} to λ_j occurred at $\lambda_{0j} = 160$ sec. to $\lambda_j = 151$ sec. at $\gamma^0 = 0.41$. This would have an obvious advantage in terms of computer time, since we will not need to reconstruct the relaxation spectrum at this moderate shear rates. In this approximated form of the model equal intervals of $\Delta \log \lambda$ is assumed even though large λ_{0j} 's are affected by relatively large γ^0 . Thus serious error may be encountered for large γ^0 as constant $\Delta \log \lambda$ will be inconsistent with the model formulation. The effect on G_j needs a little study.

From the model

$$G_{0j} = H_i \Delta \ln \lambda_j = H_i \delta \ln \lambda_j$$

At a strain input γ^0

$$x_j = 1 / (1 + \alpha_j \sqrt{N_{20j}})$$

$$G_{0i} = H_i \Delta \ln \lambda_i = H_i \delta \ln (\lambda_{0i} x_i^{1.4})$$

$$G_{0i} = G_{0i} - 1.4 H_i \delta \ln \alpha_i \sqrt{N_{20i}} \quad (56)$$

However this error term is found to be negligibly small at large λ_{0i} where the problem is centralized.

- ii. The structural character in oscillatory and steady shear

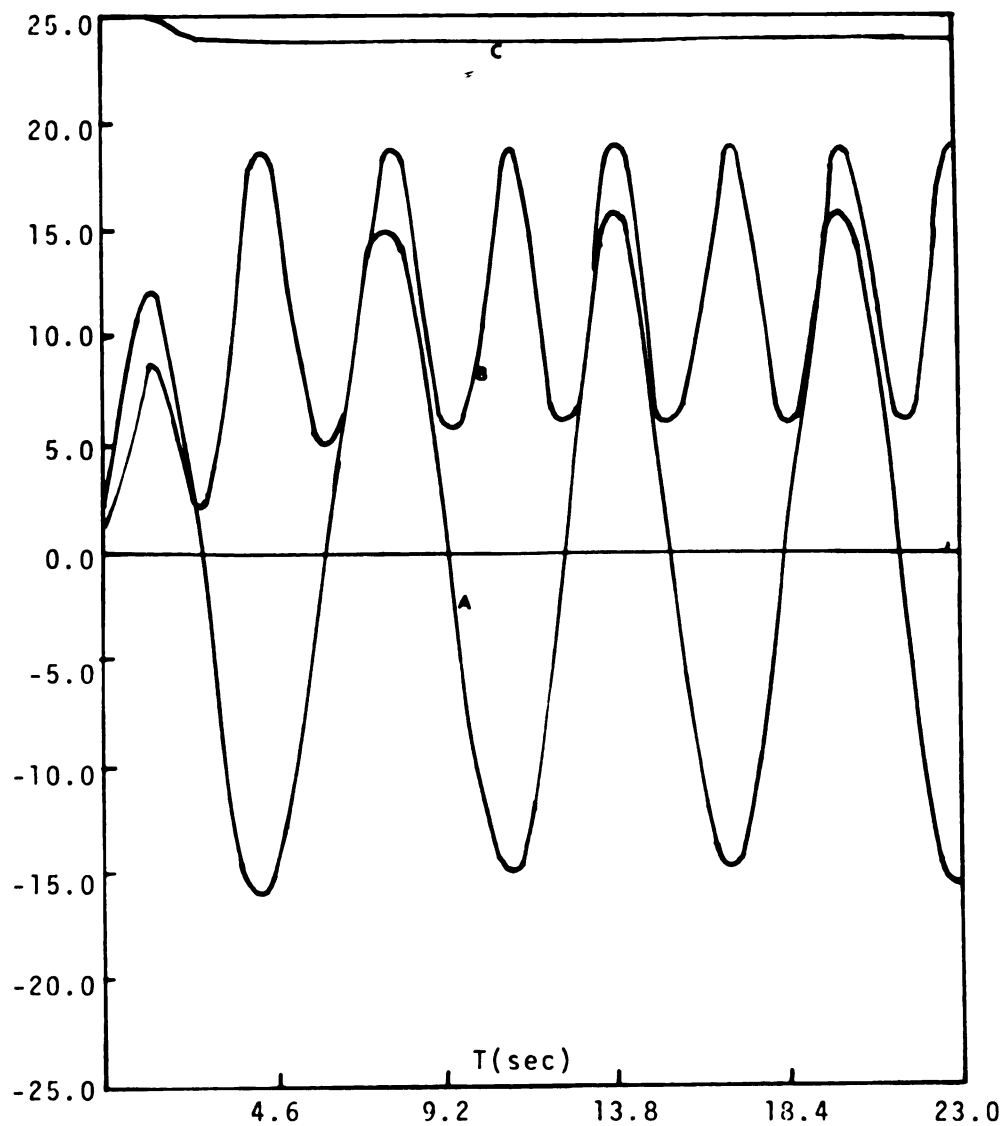
Having obtained an 'a' from the preceding section, an attempt is made here to at least study qualitatively the model's nonlinear responses of the stresses and more especially the structural parameter x_i at higher shear amplitudes. It must be pointed out also that this analysis suffers from the severe limitations we impose on the velocity gradient \underline{D} and the assumption that the contrvariant convected derivative, $\delta/\delta t$ is equivalent to the total time derivative, d/dt .

We resort to the study of spectral responses bearing in mind that the total response is the arithmetical combination of all the spectral regions that contribute significantly.

The IMSL subroutine DWGER has been employed to solve the system of ordinary nonlinear first order differential equations of eqns. 24-26. Initial values of $T_i = 0.0$, $N_i = 0.0$ and $x_i = 1.0$ and an allowable set error of 10^{-4} along with a range of the step size serves as the

input and DVOGER selects a suitable stepsize to calculate the next step which meets the error criteria. An amplitude range of 0.2 - 10.67 with relaxation times of 0.17 to 160 sec. was successfully tested. At higher ranges of relaxation times 60 sec. to 160 sec. and large amplitudes, 5.0 - 10.67, the error criteria was not met. The program is presented in the Appendix and sample computer plots are shown in Figures 7 - 11.

In Figure 7 with an input shear amplitude, x_i deviates slightly from unity and remains steady confirming the model to degenerate in a proper manner to linear viscoelasticity. The dimensionless normal stress have the expected frequency, 2ω and a pronounced displacement that has already been reported (3). In Figure 8 we notice that a 10-fold increase in the input amplitude, leads to little less than a 100-fold increase in the normal stress displacement. Christiansen and Leppard reported a correspondence of the slope equal to 2 for their solutions between the normal force displacement and the input amplitude (on a log-log scale) working however within the linear range ($\gamma_{L,0} = 1$). The x_i is seen to deviate pronoucelly from unity and exhibit a sinusoidal-like motion with a frequency of 2ω approximately. There is also a lag between x_i and N_i noting that N_i is directly the forcing function. The spectral behavior of large relaxation times e.g. $\lambda_{0i} = 37$ sec of Figure 9 is intriguing at best. The x_i curve



Y Increment B Plot 1.60 E-04

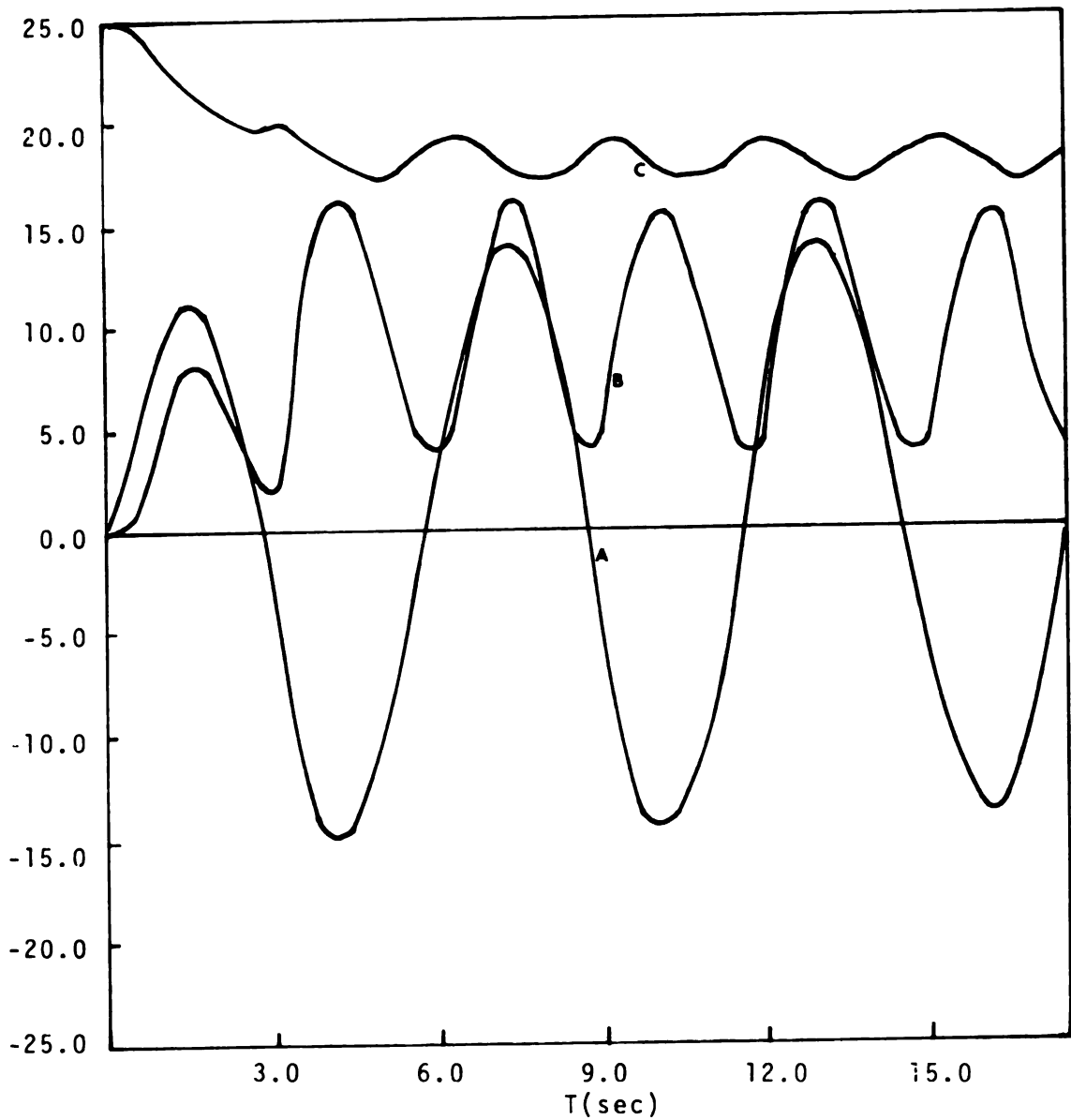
A Plot 4.00 E-03 C Plot 4.00 E--2

Figure 7. Spectral diagram of finite amplitude oscillatory shear.

(A) Dimensionless shear stress, T_i

(B) Dimensionless normal stress, N_i

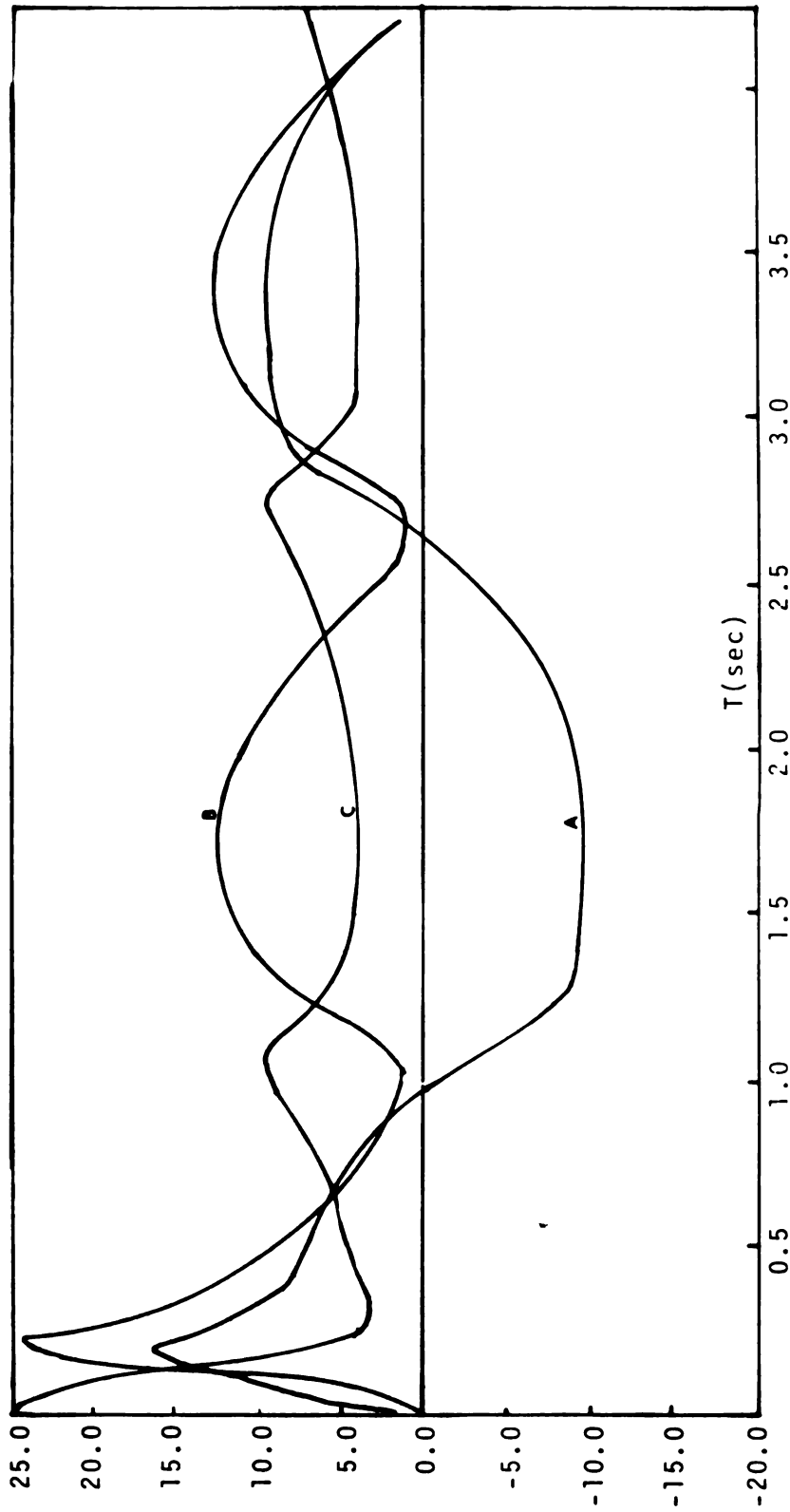
(C) Structural parameter, x_i ; relaxation time,
 $\lambda_{0i} = 1.2 \text{ sec}$ $\omega = 1.88 \text{ sec}^{-1}$, $\gamma^0 = 0.2$



Y Increment B Plot 1.600 E-02
 A Plot 4.00 E-02 C Plot 4.000 E-02

Figure 8. Spectral diagram of finite amplitude oscillatory shear

- (A) Dimensionless shear stress, T_i
- (B) Dimensionless normal stress, N_i
- (C) Structural parameter, x_i relaxation time,
 $\lambda_{oi} = 1.2 \text{ sec.}$ $\omega = 1.88 \text{ sec}^{-1}$, $\gamma^0 = 2.0$



Y Increment

B Plot 0.18E-01

A Plot 5.0E-01

C Plot 4.00 E-02

Figure 9. Spectral diagram of finite amplitude oscillatory shear

(A) Dimensionless shear stress, T_i

(B) Dimensionless normal stress, N_i

(C) Structural parameter, x_j $\lambda_{0j} = 37 \text{ sec}$, $\omega = 1.88 \text{ sec}^{-1}$, $\gamma^0 = 2.66$

rapidly drops during the transient period and dwells much longer at this low point except for sudden peaks regularly interspersed. The stress functions also lose their sinusoidal nature and only one broad peak is present in the normal stress function. These curves can be approximated by means of a Fourier analysis recognizing higher order harmonics in the shear stress and normal stress. The presence of these harmonics odd harmonics for torsion and even ones for normal force have been shown experimentally (15) and predicted by other models (e.g. the WBC & Carreau-B models) as well. This further portrays the importance of spectral studies since correlation of harmonics with experimental data may aid in choosing the correct deformation rate invariant and thus help ascertain the physical meaning of the adjustment factor, 'a'.

In Figures 10 and 11 we compare the structural parameter subjected to steady shear with that subjected to oscillatory shear. At an equivalent strain input Figure 10 shows that at the larger relaxation times more destruction of entanglements is achieved with steady shear than oscillatory shear. This is when we judge the destruction in oscillatory shear in terms of the averaged structural concentration occurring during a period of revolution. However when Figure 9 is considered it is found that the x_i function of oscillatory shear at large relaxation times behaves as though it was subjected to steady shear. We next superimpose

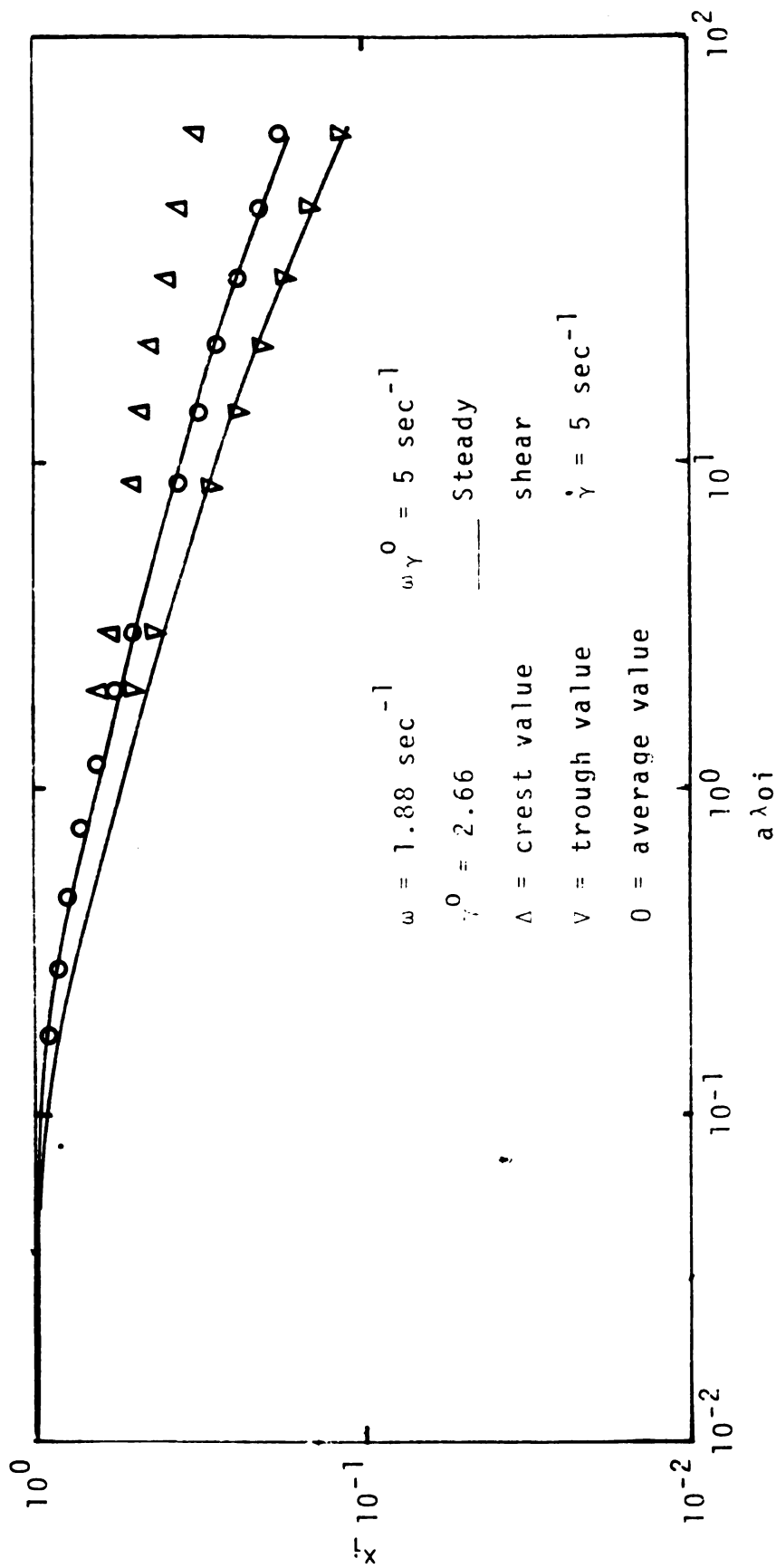


Figure 10. The oscillatory and steady structural parameters, x_j , as a function of relaxation times.

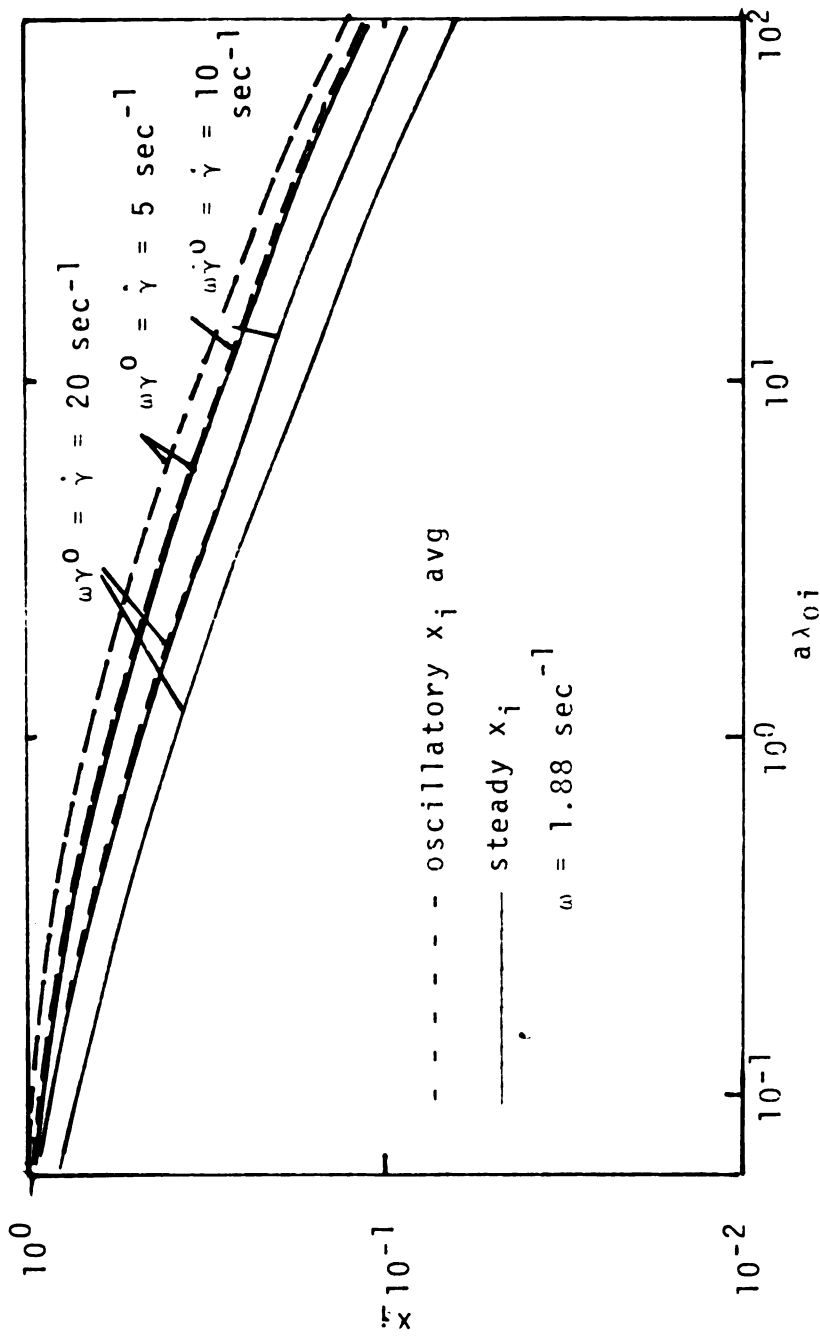


Figure 11. The oscillatory and steady structural parameters, x_i , as a function of relaxation times and shear rate.

the averaged x_i functions of oscillatory shear on their steady counterpart subjected to the same degree of strain rates as shown in Figure 11. We notice a correspondence between steady x_i and an averaged oscillatory x_i subjected to twice the strain rate of the latter. If we recognize the statement earlier made on averaged x_i at large relaxation time this correspondence is viewed with some skepticism, on the other hand such correspondence to some degree may infer that the truncated relaxation spectra of the two modes of flow are interchangeable. This further add credence to the study of large amplitude shear oscillations and it's ability to generate 'a' that can describe non-linear behavior.

iii. Shear stress growth prediction

The generalized curves of Acierno et al. (1a) for dimensionless tangential and normal stress growth in shear were utilized to obtain the shear stress and normal stress growth functions using an 'a' obtained in the preceding analysis. Since the relaxation times of polyisobutylene were used much interpolation was done to obtain the suitable parametric $a\dot{\gamma}\lambda_{0j}$ curve. However because of the regularity and smoothness of these parametric curves we feel that the associated error due to interpolation was minimal. Then $\hat{\sigma}_1(t)$ and $\hat{N}(t)$ were obtained by simply adding up all the contributions of each relaxation time at each time increment. The model results are presented

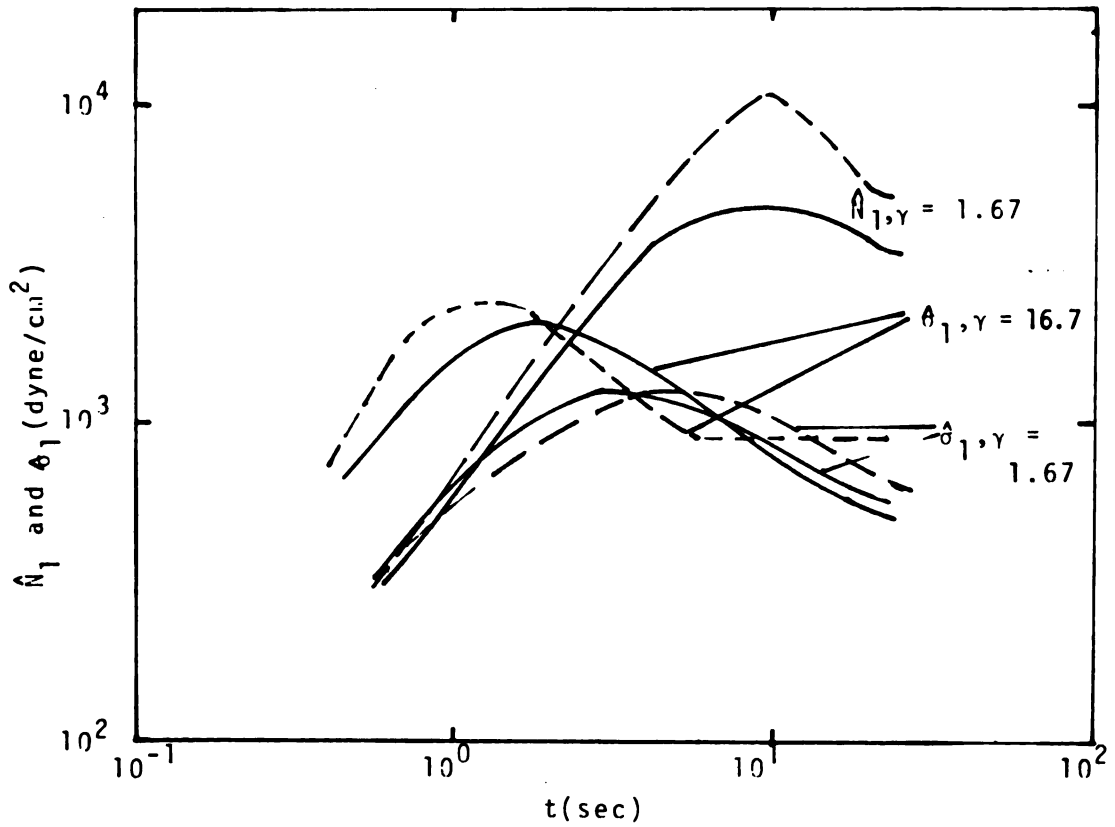


Figure 12. Shear stress and normal stress growth for 2% polyisobutylene. Data of Huppler et al. (27)
 ————— Data - - - - - Acierno model.

along with experimental data of Huppler et al. (12).

The model does a good job in predicting the magnitude of the shear stress magnitude and the time at which it occurs at a shear rate of 1.67. However at $\dot{\gamma} = 16.7$ the performance of the model is at best qualitative. For the shear stress growth function it predicts a much faster overshoot time and a larger magnitude of overshoot. It is also unable to predict the shear stress undershoot, a problem common to many acclaimed rheological models. For the normal stress growth there is a qualitative agreement between model results and data as the model tends to predict a larger overshoot than the data shows. However no conclusive judgement can be arrived at for the normal stress growth as the reliability of the data has been questioned. The reason as to why the model is unable to do a good job at high shear rates is subject to speculation, certainly we cannot blame it on the 'a' factors as the authors as well as Graessley have reported this failure even when using 'a' obtained from steady shear.

DISCUSSION

Acierno et al. evaluated the adjustable parameter 'a', from steady shear and normal stress data. With the single value of a, they obtained a good fit of data over a shear rate range of 1×10^{-4} to $1 \times 10^3 \text{ sec}^{-1}$ on low density polyethylene melts. On the other hand Graessley et al. working on 8% and 12% polystyrene solutions could predict steady shear stress data only by choosing several values of 'a'. For the 8% solution the values required ranged from 0.2 at $\dot{\gamma} = 0.1 \text{ sec}^{-1}$ to 0.5 at $\dot{\gamma} = 100 \text{ sec}^{-1}$. For the 12% solution from 0.4 to 0.9 in same range of shear rates. They were then able to predict stress growth data by choosing an a which gave the best fit with steady shear data at the particular shear rate. From Figure 2 we found that 'a' obtained from finite amplitude oscillatory shear data successfully fit data with a shear rate range of 0.001 sec^{-1} to 0.3 sec^{-1} . Also with this 'a' quantitative prediction of stress growth data at $\dot{\gamma} = 1.67 \text{ sec}^{-1}$ was obtained. This perhaps indicate the usefulness of non-linear oscillatory data as far as the determination of 'a' is concerned.

Another severe test of the Acierno model is met when predicting stress growth data at large shear rates. In

comparing the model predictions with the Carreau-B model (22) predictions on the same fluid, there is a striking resemblance between both model results at a shear rate of 16.7 for shear stress growth. Both quantitatively disagree with data predicting too early a time for overshoot, much larger magnitude and a complete absence of undershoot. The Carreau-B model, a modification of the Bird-Carreau model is similarly based on network theory however differs strategically from Acierno's as it relates the destruction of network junctions to the second invariant of the rate of strain. In the Acierno model it is noticed that at very small times after the onset of shear, the shear stress contributions of much of the spectral regions (except larger relaxation zones) arise close to the overshoot of the stress curve associated to this unit. This conceptually appears as if destruction of the network junctions on each spectral zone is instantaneous. By choosing a different 'a' say, these spectral curves are only shifted vertically and even though the total result may correctly predict the maximum observable overshoot it will still incorrectly determine overshoot time.

We thus speculate that the invariant used in the generalization of $\dot{\gamma}$ in the destruction term of the structural variable equation is much too severe and suggest a combination of the invariant of the extra stress and of the strain rate be used. This similar conclusion has been

arrived at by Carreau (22). In this work the predictive capability of Acierno model with the parameter obtained from oscillatory shear of the normal stress functions is only seen in the normal stress growth prediction. The fact that same qualitative agreement is met adds credence to the 'a' evaluation. Claims made in this study for 'a' is restricted to 2% polyisobutylene solution in Primol 355.

CONCLUSION

It has been shown in the preceding pages that the adjustment parameter 'a' of the Acierno rheological equation of state can be obtained reliably and uniquely from large amplitude shearing experiments. The computed results further show in agreement with McDonald's observation that $G'(\omega, \gamma^0)$ should be the choice correlation function as it expresses more nonlinear characteristics of the viscoelastic fluid in oscillatory shearing. However the 'a' obtained from $G'(\omega, \gamma^0)$ correlation unsuccessfully predicted $\eta'(\omega, \gamma^0)$ between $\gamma^0 = 0.1$ to 1.28. For the $\eta'(\omega, \gamma^0)$ prediction an 'a' of 0.1 and 0.2 were required to fit data at $\omega = 0.188$ and 1.88 sec^{-1} respectively.

A method of numerical solution of the Acierno model in large amplitude oscillatory shearing where harmonics becomes significant has been outlined. Due to the lack of data in this region, no numerical predictions have been given, however we noted a similar behavior between junction concentrations of the large relaxation zones to similar concentrations subjected to steady shear. With a single 'a' value the model is quantitatively unable to predict shear growth data at high shear rates. For polyisobutylene solution at high shear rates the model predicts an earlier

and larger overshoot and no undershoot in the stress growth function. In view of these failings much more tests at larger shear rates and amplitudes and different flow regimes with different polymeric fluids will be needed to establish the singularity of 'a'.

NOMENCLATURE

NOMENCLATURE

A_n	Def. by eqn. 38a Adjustment (Acierno model) parameter
$A'_i, A_{n,i}$	Fourier coefficients def. by eqn. 27 & 29
$B_i, B_{n,i}$	Fourier coefficients def. by eqn. 27 & 29
B_n	def. by eqn. 38b
\underline{C}	Cauchy Tensor = $\frac{\delta x^m}{\delta x^i} \frac{\delta x^n}{\delta x^j} g_{mn}(x')$
\underline{C}^{-1}	Finger Tensor = $\frac{\delta x^i}{\delta x^m} \frac{\delta x^j}{\delta x^n} g^{mn}(x')$
$C'_{oi}, C_{on,i}$	Fourier coeffs. def. by eqns. 28 & 30
$D'_i, D_{n,i}$	Fourier coeff. def. by eqns. 28 & 30
d_{ij}	Primary normal stress displacement, dynes/cm ²
$E'_i, E_{n,i}$	Fourier coeff. def. by eqns. 28 & 30
E	Elastic energy, (erg/cm ³)
F	Total axial force, dynes
G'	Storage modulus, dynes/cm ²
G''	Loss modulus, dynes/cm ²
g_{mn}, g^{mn}	Components of the metric tensor
H	Spectrum density, dynes/cm ²
i	$\sqrt{-1}$
N_i	Dimensionless normal stress, eqn. 23b
\hat{N}_1	Primary normal stress component following shear growth, dynes/cm ²

R	Radius of cone and plate, cm
R_e	Real part of a complex number
t	Current time
t'	Past time
T	Torque transmitted through the fluid, dynes/cm
\underline{v}	Velocity tensor, cm/sec
x	Structural parameter (Acierno model)
x^i, x^j	Coordinates of a fluid particle at time t
x^i, x^j	Coordinates of a fluid particle at time t'

Greek symbols

α_i	Def. by eqn. 23a
α_j	Bird-Carreau model parameter
β_j	Dimensionless frequency
ϵ	Bird-Carreau model parameter
$\gamma_{\theta\phi}$	$\theta\phi$ -component of finite strain tensor
$\gamma_{\theta\phi}^0$	$\theta\phi$ -component of the strain rate tensor, sec^{-1}
γ^0	Strain amplitude
$\dot{\gamma}^0$	Strain rate amplitude, sec^{-1}
$\dot{\gamma}$	Shear rate, sec^{-1}
δ_j	Phase shift between strain rate and shear stress, rad.
λ_{0i}	Equilibrium relaxation time, sec
λ_j	Bird Carreau and Acierno model relaxation times, sec
λ_{in}	Bird-Carreau model parameters, sec

μ	Bird-Carreau model memory function
η	Viscosity, poise
η'	Dynamic viscosity, real part of complex viscosity
η''	Imaginary part of complex viscosity, poise
η_0	Zero shear rate limiting value of viscosity, poise
ψ_0	Angle of cone ($<4^\circ$), degrees
θ^*	Complex primary normal-stress-difference coefficient dynes sec^2/cm^2
θ'	Real part of θ^* , dynes sec^2/cm^2
θ''	Imaginary part of θ^* , dynes sec^2/cm^2
θ^d	Primary-normal-stress-difference-displacement coefficient, dynes sec^2/cm^2
θ_t	Dimensionless time, def. by eqn. 23a
$\underline{\underline{\tau}}$	Shear stress tensor, dynes/ cm^2
$\tau_{ij}, \tau^{ij}, \tau^{ii}$	Component of shear stress tensor, dynes/ cm^2
ω	Frequency of strain oscillation, rad/sec
\parallel	Second flow invariant = $(\dot{\underline{\underline{y}}}: \dot{\underline{\underline{y}}})$

Errata

$G(t)$	Steady elastic modulus, dynes/ cm^2
G_i	Dynamic nonlinear elastic modulus, dynes/ cm^2
G_{0i}	Dynamic equilibrium elastic modulus, dynes/ cm^2
σ	Steady first normal stress, dynes/ cm^2
δ_1	Shear stress component following shear growth, dynes/ cm^2

APPENDIX

```

PROGRAM LSQS(INPUT,OUTPUT)
C THIS PROGRAM EMPLOYS THE ROUTINE ICVKU(IMS), DESIGNED TO COMPUTE A
C LEAST SQUARES CUBIC SPLINE APPROX. TO A SET OF POINTS. THE CUBIC
C SPLINE APPROX. HAS A FIXED NO. OF KNOTS, BUT THE KNOT LOCATIONS ARE
C DETERMINED BY ICVKU IN ORDER TO MINIMIZE THE LEAST SQ. ERROR. THE
C PROGRAM THEN GENERATES THE SPLINE FUNCTION, S, ITS 1ST. DERIV., S**1, THE
C 2ND. DERIV., S**2, AT DATA POINTS AND OUTPUTS HQ(L)=Q(S**1,S**2)
C
C DIMENSION X(16),F(16),XI(16),XK(4),Y(3),C(3,3),AK(16),
4Z(40),DZ(40),DZ2(40),HA(40),
5RL(16),S(60),DS(60),DDS(60),HC(60),G(16),ALAM(60),ACC(16),AFC(60)
C DATA 77820.,6000.,1810.,1410.,850.,60.,420.,320.,220.,180.,137.,
2130.,90.,79.,47.,32.7
C DATA XL7.0319.,C15.,05.,075.,13.,2.,3.,4.,6.,75,1.3,1.6,2.,2.6,4.,
46.,7
DO 5 I=1,16
F(I)=S(I)*X(I)
X(I)=ALAM(X(I))
IC=3
NYK=4
C
C.....INITIAL KNOT LOCATION.....
C
XK(1)=X(1) XK(2)=X(9) XK(3)=X(13) XK(4)=Y(10)
NX=16
CALL ICVKU(X,7,X,XK,NYK,Y,C,IC,FRFRK,FM,TER)
I=1
DO 40 J=1,16
IF(X(J).EQ.XK(2))I=2
IF(X(J).EQ.XK(3))I=3
S(J)=C(1,3)*(X(J)-XK(I))**3+C(1,2)*(X(J)-XK(I))**2+C(1,1)*(X(J)-
1Y(I))+Y(I)
C
C.....COMPUTATION OF INITIAL HQ AT DATA POINTS.....
C
DS(J)=3.*C(1,3)*(X(J)-XK(I))**2+2.*C(1,2)*(X(J)-XK(I))+C(1,1)
DDS(J)=6.*C(1,3)*(X(J)-XK(I))+2.*C(1,2)
RI(J)=SQRT(5.)/XK(I)
HQ(J)=.6356*(S(J)-4./3.*DS(J)+DDS(J)/3.)
40 CONTINUE
PRINT 15,IFR,ERROR
15 FORMAT(1X,IFR=,13,10X,FRFRK=,13)
PRINT 20,(XK(J),J=1,4)
20 FORMAT(7/2X,F10.4)
PRINT 30,(Y(J),J=1,3)
30 FORMAT(7/2X,F10.4)
PRINT 35,(C(I,J),I=1,3),J=1,5)
35 FORMAT(7/1X,3F10.4)
PRINT 70
70 FORMAT(7/1X, CURVE FITTING HQ USING LEAST SQUARE APPROX. BY CUBIC
SPLINE WITH VAR. KNOTS)
PRINT 75
75 FORMAT(7/5X, G**1,13X, OVERALL,7X, LAM,1F10.4,LAMBDA,10X, C,10X, DS,
+DZ,10X, DZ2/DL,2*,10X, H**2)
PRINT 100,(F(J),XL(J),X(J),RL(J),S(J),DS(J),DDS(J),HQ(J),J=1,16)
100 FORMAT(7/1X,8F15.4)
C
C.....COMPUTATION OF INITIAL HQ AT MORE (NON-DATA) POINTS TO BE
C.....USED FOR ITERATION.....
C
DO 11 J=1,33
A-C(J)=SQRT(5.)/ALAM(J)
11 A-C(J)=ALAM(A-C(J))
I=1
DO 22 J=1,33
IF(A-C(J).EQ.XK(2))I=2
IF(A-C(J).EQ.XK(3))I=3
Z(J)=C(1,3)*(A-C(J)-XK(I))**3+C(1,2)*(A-C(J)-XK(I))**2+C(1,1)*(A-C
E(J)-XK(I))+Y(I)
DZ(J)=3.*C(1,3)*(A-C(J)-XK(I))**2+2.*C(1,2)*(A-C(J)-XK(I))+C(1,1)
DZ2(J)=6.*C(1,3)*(A-C(J)-XK(I))+2.*C(1,2)
22 HA(J)=.6356*(Z(J)-4./3.*DZ(J)+DZ2(J)/3.)
PRINT 12,(ALAM(J),A-C(J),A-C(J),Z(J),DZ(J),DZ2(J),HA(J),J=1,33)
120 FORMAT(7/1X,7F15.4)
END
*END

```

PROGRAM LSQSF

List of Principal Variables

ALAM	Relaxation time, at inserted points
AWC	$\log \omega_c$
C	Spline coefficient (output). C is an N XK-1 by 3 matrix
DS, DDS	First and 2nd derivative respectively of the spline function at the data points
DZ, DDZ	First and 2nd derivative respectively of the spline function at the inserted points.
F	The dynamic loss modulus (or function values) $G'' = \omega \eta'$
G	The dynamic viscosity, η' (Input)
HO	The unrefined relaxation density at data points
HA	The unrefined relaxation density at inserted points
IC	Row dimension of matrix C in the calling program (input)
I,J,K	i,j,k, counters
NX	Number of data points
NXK	Number of knot locations
RL	$= \sqrt{5}/\omega$, equilibrium time constants at data points
S	Spline function at data points
XK	Knot location
XL	The frequency of oscillation (data for inserted points), abscissa

X = $\log x_1$
Y Vector of length $NXK-1$ (output)
WC Frequency of oscillation (data for inserted points), abscissa
WK Work area
Z Spline function at inserted points

```

PROGRAM CREDIT(INPUT,OUTPUT)
C THIS PROGRAM USES THE INITIAL RELAXATION SPECTRUM DATA FROM THE
C PROGRAM LSGSF AND BY COMPARING WITH OBSERVED G*(U) ON INPUT
C ITERATES FOR H1 WHICH GIVES SATISFACTORY THEORETICAL VALUES OF
C G*(U). A SIMPLE APPROXIMATION SCHEME IS USED.
C
C DIMENSION HG(40),ALAM(40),S(40),H1(40),GC(40),DIFF(40),HC(40)
C 2,RLAM(40)
C DATA ALAM /900.,760.,600.,440.,375.,295.,230.,180.,140.,110.,90.,70
C 6.,53.,41.,27.5,20.5,20.,15.,12.,9.5,7.2,5.8,4.5,3.6,2.8,2.1,1.7,
C 61.34,1.05, .82, .64, .5, .39/
C DATA S/17.7, 21.5, 27.9, 30.2, 32.7, 41.4, 47.6, 54., 61.7, 67.3, 73.4, 80.3
C 4,86.9, 93.4, 99., 104., 109., 114., 118., 121., 124., 127., 131., 135., 142.,
C 5149., 158., 164., 171., 181., 188., 195., 202./
C DATA H1/2.10, 1.85, 2.24, 2.15, 4.73, 6.8, 9.44, 12.5, 16., 19.7, 27.4, 29.,
C 43.2, 37.3, 41.8, 46.5, 51.1, 55.8, 60.7, 65.9, 70.9, 71.6, 72.1, 71., 71., 71., 72
C 9.4, 74.8, 77.9, 81.9, 85.6, 91.8, 97.3, 103.5/
C ITER=0, ITEL=10, IITMAX=40
C
C .....REORDERING OF THE RELAXATION TIMES.....
C
C DO 7 J=1,33
C RLAM(J)=ALAM(J)/SQRT(S(J))
C C(J)=1./RLAM(J)
C CONTINUE
C
C .....COMPLETE G*(U) CALC.....
C
C DO 21 K=1,33
C 21 GC(K)=0.0
C 11 DO 51 J=1,33
C GC(K)=0.0
C DO 47 J=1,33
C GC(K)=GC(K)+HG(J)*RLAM(J)* C(K)*.24 / (1.+(KC(K)+RLAM(J))*C)
C 47 CONTINUE
C 51 CONTINUE
C
C .....ITERATION SCHEME TO OBTAIN FINAL H1.....
C
C ITER=ITER+1
C IF(ITER.LE.7) PRINT*,C, GC(J),S(J),GC(J),H1(J),J=1,33
C 4 FORMAT(4F15.3)
C IF(ITER.GT.IITMAX) GOTO 29
C DO 61 J=1,33
C H1(J)=HG(J)*S(J)/GC(J)
C DIFF(J)=ABS(H1(J)-H1(J))
C 61 CONTINUE
C
C .....A CHECK FOR CONVERGENCE.....
C
C COMP=DIFF(1)
C DO 28 I=2,33
C COMP=AMAX1(COMP,DIFF(I))
C 28 IF(COMP.LE.TOL)GOTO 98
C DO 11 J=1,33
C HC(J)=H1(J)
C GOTO 11
C 98 PRINT 15
C 100 FORMAT(7X, 'LAMBDA', 5X, 'S', 10Y, 'GC', 10X, 'H1')
C PRINT 100, (RLAM(J), S(J), GC(J), H1(J), J=1,33)
C 100 FORMAT(4F15.4)
C PRINT 12, ITER
C 120 FORMAT(7X, 'NO. OF ITER=', I2)
C STOP * RUN *
C 98 PRINT 111
C 111 FORMAT(77X, 'NO CONVERGENCE OBTAINED')
C END
C
C *****

```

```

PROGRAM LIV(INPUT,OUTPUT)
DIMENSION K(20),ALC(20),ETAP(10),SLP(10),GDP(10),ETAP(10)
DATA W/.0019,.0026,.045,.075,.13,.2,.3,.4,.5,.75,1.3,1.9,2.8,4.0,5.0,50.5/
DATA ETAP/ 8000.,6000.,1800.,1400.,850.,500.,400.,320.,200.,100. /
4100.,100.,80.,70.,47.,32./
DATA W/(227.7,100.9,54.5,43.6,41.6,39.8,37.6,36.6,36.0,34.7,29.1,
423.8,18.8,14.4,11.4/
DATA ALC/ .17,.28,.46,.74,1.2,2.0,3.2,5.2,7.5,14.,23.,37.,50.,79.,115. /
50./
DATA GDP/ 70.,60.,50.,120.,150.,160.,210.,180.,260.,280.,300.,320.,
4300.,350.,400.,450./
DO 5 J=1,10
ETAP(J)=0.0
GDP(J)=0.0
DO 10 K=1,10
DO 7 I=1,15
ETAP(K)=ETAP(K)+G(I)*ALC(I)/(1.+(ALC(I)+G(I)))**2)
CONTINUE
10 CONTINUE
DO 20 J=1,16
DO 15 I=1,14
GDP(J)=GDP(J)+W(I)*(ALC(I)+G(J))**2/(1.+(ALC(I)+G(J)))**2)
15 CONTINUE
20 CONTINUE
PRINT 30
30 FORMAT(/'X',10,'X',ETAP(1),5X,ETAP(2),5X,ETAP(3),5X,ETAP(4),5X,ETAP(5),5X,ETAP(6),5X,ETAP(7),5X,ETAP(8),5X,ETAP(9),5X,ETAP(10))
PRINT 40,(G(J),ETAP(J),ETAP(J),GDP(J),GDP(J),J=1,10)
40 FORMAT(2X,5F3.4F11.2)
END

```

PROGRAM CUFIT AND LINV

List of Principal Variables

ALAM	Relaxation times obtained from program LSQSF (input)
DIFF	Absolute difference between $H(\)$ and $H(\)$
GC	The calculated storage modulus obtained from H
H	Unrefined relaxation density obtained from program LSQSF (input)
H	Final relaxation density, (output)
RLAM	Recorded relaxation times used by CUFIT
S	Observed storage modulus
WC	The frequency calculated from RLAM

PROGRAM LINV

ALO	Final and refined relaxation times (input)
ETAP	The calculated dynamic viscosity at data points (output)
ETAPO	The observed dynamic viscosity at data points (input)
GDP	The calculated dynamic storage modulus at data points (output)
GDPO	The observed dynamic storage modulus at data points (input)
GO	Final and refined elastic modulus (input)
W	The frequency of oscillation at data points (input)


```

C.....COMPARE Gm OBSERVED AND Gm CALCULATED.....
C
  DIFF(I,K)=ABS((RGNO(I,K)-RGN(I,K))/RGNO(I,K))
43  CONTINUE
C
C.....COMPUTE NONLINEAR DYNAMIC VISCOSITY.....
C
  DO 82 K=1,10
    EPN(I,K)=0.0
    DO 86 L=1,15
      EPN(I,K)=EPN(I,K)+GG(L)*ALP(L)*(1.+A(N)*GAM(I,K)+B(I,L)*SQRT(ANNO
7(K,L)))+.4/(1.+A(N)*GAM(I,K)+SQRT(ANNO(K,L))+B(I,L))+2.8*B(I,L)
2**2)
84  CONTINUE
    REP(I,K)=EPN(I,K)/EPL(I)
82  CONTINUE
    PRINT 75,I(I),A(N)
75  FORMAT(/5X,2=,F6.3,5X,4=,F4.2)
    PRINT 125
125  FORMAT(/5X,4=INITIAL APPROX OF N20)
    PRINT 13,((AND(L,K,1),K=1,15),L=1,10)
    PRINT 126
126  FORMAT(/5X,4=FINAL N20 OBTAINED BY SUCCESSIVE APPROX. WITH THE ADDI
4TION OF ALPHA)
    PRINT 13,((ANNO(L,K),K=1,15),L=1,10)
    PRINT 15,((EPN(I,K),EPN(I,K),TETN(I,K),K=1,10)
13  FORMAT(/5X,15F6.4)
15  FORMAT(/7F15.4)
    PRINT 91
    PRINT 100
91  FORMAT(/7X,4= GAMMA,5X,4= G(G,W)/G(W),5X,4= G(G,W)/G(W),5X,4= DIFF
4=,5X,4= ETAN(G,W)/ETAN(W),5X,4= TETAD(G,W)/TETAD(W))
100  FORMAT(10X,4= CALC,14X,4= OLS,22X,4= CALC,14X,4= CALC)
    PRINT 88,((GAM(I,J),RGN(I,J),RGNO(I,J),DIFF(I,J),REP(I,J),RTETN(I
5,J),J=1,10)
88  FORMAT(/F10.2,5F15.3)
    N=N+1
    IF(N.GT.4) GOTO 102
    GOTO 2
102  I=I+1
    L=1
    IF(I.GT.2) GOTO 126
    GOTO 2
126  CONTINUE
7  FORMAT(/5X,4=AN ELEMENT(S) OF AND DOES NOT CONVERGE)
    END
*END

```

PROGRAM LAMVIS

List of Principal Variables

A	The adjustment parameter
ALO	The equilibrium relaxation times
ANO	The linear dimensionless normal stress function
ANNO	Nonlinear dimensionless normal stress function
B	Dimensionless frequency
DIFF	Percent difference
EPL	Linear dynamic viscosity
EPN	Nonlinear dynamic viscosity
GO	Equilibrium elastic modulus
GPL	Linear dynamic storage modulus
GPN	Nonlinear dynamic storage modulus
I,J,K,L	i,j,k,l, counters
REPN	Normalized nonlinear dynamic viscosity
RGN	Normalized nonlinear storage modulus
RGNO	Normalized observed nonlinear storage modulus
W	The frequency of oscillation

PROGRAM SONODE

List of Principal Variables

A	Ratio of strain amplitude supplied by input
ALO	The relaxation time
B	The dimensionless frequency
DFUN	External supplied subroutine required by DVOGER
DVOGER	IMSL subroutine, first order differential equation solver
DY	The differential function for input system of differential equation required by DFUN
EPS	Specification of the maximum error criterion
ERROR	Contains the estimated one step error in each component on output
H	On input, suggests the step size to be attempted on the next step
HMAX	On input, the largest step size allowable in this integration
HMIN	On input, the smallest step size allowable in this integration
I	Counter for A
J	Number of time steps in DVOGER
JSTART	Initializes the integration
MAXDER	Maximum order to be used in the approximation
M	Number of ordinary differential equations
MTH	Method indicator
WK	Work area

- T On input contains the initial time, on output
 contains the updated value of time using H as
 the increment
- Y Y is two dimensional array (8 by M) containing
 the dependent variables
- YMAX Set in input is the suggested maximum absolute
 value of each component of the dependent
 variable calculated so far

REFERENCES

REFERENCES

- 1a. D. Acierno et al., Journal of Non-Newtonian Fluid Mechanics, 1, 125-146 (1976).
- 1b. I.F. MacDonalds et al., Chem. Engineering Science, 24, 1615-1625 (1969).
1. J.D. Ferry, Viscoelastic Properties of Polymers, J. Wiley and Sons, New York, 1970.
2. D.C-H. Cheng, British Journal of Applied Physics, 17, 253 (1966).
3. E.B. Christiansen et al., Trans. Soc. Rheol., 18, 65-86 (1974).
4. T.W. Spriggs et al., Trans. Soc. Rheol., 10, 191-213 (1966).
5. A.S. Lodge, Rheol. Acta, 7, 379 (1968).
6. W.W. Graessley et al., 16, 291-301 (1977).
7. D. Cross, K. Jayaraman, J. Przybyla, Work yet published.
8. D. Acierno et al., J. Non-Newtonian Fluid Mech., 1, 147 (1976).
9. I-Jen Chen et al., Trans. Soc. Rheol., 16, 59-78 (1972).
10. J. Meissner, Rheol. Acta, 10, 230 (1970).
11. Ch. Goldstein et al., Rheol. Acta, 12, 253-262 (1973).
12. J.D. Huppler et al., Trans. Soc. Rheol., 11, 181-204 (1967).
13. J.H. Oldroyd, Proc. Roy. Soc. (London) A245, 278 (1958).
14. K. Walters, Rheometry, Chapman & Hall (London), 1975, p. 120.
15. J. Harris et al., Rheol. Acta., 6, 3 (1967).

16. W. Philippoff, *Trans. Soc. Rheol.*, 10, 317-334 (1966).
17. Tee and Dealy, *Trans. Soc. Rheol.*, 19, 595-615 (1975)
18. J.S. Dodge et al., *Rheol. Acta*, 8, 480 (1969).
19. R.B. Bird and P.J. Carreau, *Chem. Engng. Sci.*, 23, 901 (1968).
20. E. Ashare, *Trans. Soc. Rheol.*, 12, 535 (1968).
21. N.W. Tschoegl, *Rheol. Acta*, 10, 582-594 (1971).
22. P.J. Carreau, *Trans. Soc. Rheol.*, 16, 99-127 (1972).

